UCRL-53645
Distribution Category UC-11

UCRL--53645

DE8 006145

Hydrothermal Interaction of Solid Wafers of Topopah Spring Tuff with J-13 Water and Distilled Water at 90, 150, and 250°C, Using Dickson-Type, Gold-Bag Rocking Autoclaves

K. G. Knauss, W. J. Beiriger,

D. W. Peifer, and A. J. Piwinskii

Manuscript date: September 1985

LAWRENCE LIVERMORE NATIONAL LABORATORY
University of California • Livermore, California • 94550

Available from National Technical Information Service • U.S. Department of Commerce
5285 Port Royal Road • Springfield, VA 22161 • A03 • (Microfiche A01)

Contents

Hydrothermal Interaction of Solid Wafers of Topopah Spring Tuff with J-13 Water and Distilled Water at 90, 150, and 250°C, Using Dickson-Type, Gold-Bag Rocking Autoclaves

Abstract

The Nevada Nuclear Waste Storage Investigations Project has conducted experiments to study the hydrothermal interaction of rock and water representative of a potential high-level waste repository at Yucca Mountain, Nevada. The results of these experiments help define the near-field repository environment during and shortly after the thermal period that results from the emplacement of nuclear waste. When considered in conjunction with results contained in companion reports, these results can be used to assess our ability to accelerate tests using the surface area/volume parameter and/or temperature.

These rock-water interaction experiments were conducted with solid polished wafers cut from both drillcore and outcrop samples of Topopah tuff, using both a natural ground water and distilled water as the reacting fluid. Pre- and post-test characterization of the reacting materials was extensive. Post-test identification and chemical analysis of secondary phases resulting from the hydrothermal interactions were aided by using monoliths of tuff rather than crushed material. All experiments were run in Dickson-type, gold-bag rocking autoclaves that were periodically sampled at *in situ* conditions. A total of nine short-term (up to 66-day) experiments were run in this series; these experiments covered the range from 90 to 250°C and from 50 to 100 bar. The results obtained from the experiments have been used to evaluate the modeled results produced by calculations using the geochemical reaction process code EQ3/6.

Introduction

The Nevada Nuclear Waste Storage Investigations (NNWSI) Project is studying the suitability of the Topopah Spring Member of the Paintbrush Tuff (Tpt) as a potential site for a high-level waste (HLW) repository at Yucca Mountain. Before an appropriate waste package can be designed, however, it is necessary to understand the near-field environment surrounding the waste package.

The anticipated repository conditions and an estimate of the upper bounds on exper nental conditions appropriate for unanticipated but possible scenarios based on repository- (Travis et al., 1984) and package- (Stein et al., 1984) scale thermal modeling have been presented briefly in a companion report on crushed tuff experiments (Knauss et al., 1985). The conditions for experiments described in this report cover the range of estimated anticipated and unanticipated temperatures. The experiments were done under fully saturated conditions, however, with higher fluid-to-solid ratios than anticipated and were run at pressures sufficient (at least 50 bar) to ensure the presence of only liquid water at all temperatures.

Most hydrothermal interaction experiments used tuff taken from drillcore USW G-1, at a depth equivalent to that of the potential repository beneath Yucca Mountain; tuff sampled from an outcrop at a slightly higher stratigraphic position in the Tpt section was also used in a few experiments. The mineralogy, geochemistry, and physical properties of these outcrop samples are similar to those from the potential repository depth (Knauss, 1984). Natural water from a nearby well (J-13), which produces water largely from the Tpt, was used as the primary reacting fluid. Several experiments were also run using distilled water as the reacting fluid to assess the effects of the starting fluid composition on the steady-state water composition achieved as a result of hydrothermal interaction.

Dickson-type, gold-bag rocking autoclaves were used for these hydrothermal interaction experiments (Seyfreid et al., 1979). These autoclaves were designed to allow repeated fluid sampling at *in situ* conditions without perturbing the experiment. Preliminary experiments using only outcrop wafers and J-13 water run in static, Teflon-lined autoclaves were described by Knauss and Beiriger (1984a).

The experiments using solid polished wafers of tuff were run for up to 66 days. The use of these solid wafers allowed the run products from the hydrothermal interaction to be observed and analyzed directly. However, the wafers slowed the rate of reaction because of a decreased solid surface area/solution volume ratio (SA/V). Analogous experiments using crushed drillcore and outcrop tuff (Knauss et al., 1985) had significantly higher SA/V ratios;hence, the evolution of the fluid-phase composition was accelerated. In this sense, the two sets of experiments were complementary.

This report presents the results of fluid sample analyses taken during the course of the tuff-water reaction at 90, 150, and 250°C and low pressure (50 and 100 bar). The conditions for each experiment are summarized in Table 1. The detailed post-test solid-phase analyses emphasize run product compositions. Phase characterization was accomplished with scanning electron microscope/electron microprobe (SEM/EMP) analysis, using qualitative energy-dispersive spectrometry (EDS) techniques and,

Table 1. Experimental conditions for experiments with tuff and water (DI = distilled water).

Experiment	Solid	Treatment	Fluid	Temp. (°C)	Pressure (bars)	Duration (days)
DB6	Tpt FR	Polished wafer wash DI	J-13	150	100	64
DB7	Tpt FR	Polished wafer wash DI	J-13	250	100	64
DB8	Tpt G-1 1232 ft	Polished wafer wash DI	J-13	150	50	66
DB9	Tpt G-1 1232 ft	Polished wafer wash DI	J-13	250	50	66
DB14	Tpt G-1 1232 ft	Polished wafer wash DI	J-13	90	50	49
DB16	Tpt G-1 1232 ft	Polished wafer wash DI	DI	150	100	64
DB17	Tpt G-1 1232 ft	Polished wafer wash DI	DI	90	100	64
DB18	None	None	J-13	90	50	52
DB19	None	None	J-13	150	50	52

where possible quantitative wavelength-dispersive spectrometry (WDS). Phase identification was based on x-ray diffraction (XRD) techniques. Post-test quantitative WDS analyses of the primary phases (phenocrysts and matrix) are also presented.

Starting Materials

The reacting fluid used in most of our experiments is well J-13 water. This natural ground water is used by the NNWSI Project as the reference water for waste package experiments. The method by which it is collected and used was described by Knauss et al. (1985). The average composition of this water, as analyzed in many waste package experiments, is contained in Table 2 (Delaney, 1985). An analysis of the J-13 water actually used in individual experiments was made at the start of each experiment. This value is represented as Day 0 in all fluid composition data tables and plots. An analysis of the composition of the distilled water used in two of the experiments (DB16 and DB17) is provided as the Day 0 sample in the appropriate tables and plots.

The reacting solid used in most of our experiments is a densely welded, devitrified ashflow tuff (Tpt) taken 1232 ft below the surface from drill hole USW G-1. This tuff has been characterized in some detail by Knauss et al. (1985). The analyses in the Knauss report include petrographic examination, XRD, neutron activation analysis (NAA), mercury porosimetry, and gas adsorption BET surface analysis. Also included is a comparison with samples collected at nearby intervals from hole G-1 (Bish et al., 1981; Warren et al., 1984). The reader is referred to these documents for more detail. The results of quantitative analyses of both thin sections and polished wafers of the USW G-1 1232 material, as obtained with EMP/WDS techniques, are given below.

Table 2. Average composition of J-13 water (Delany, 1985).

Species	Concentration (ppm)
SiO_2	57.8
pH	7.6
HCO_3	125.3
F	2.2
Cl	6.9
NO_3	9.6
SO_4^{-2}	18.7
Al^{+3}	0.012
$B(OH)_3$	0.128
Fe^{+2}	0.006
Ca^{+2}	12.5
Mg^{+2}	1.92
K	5.11
Na	43.9
Li	0.042
Charge balance	0.18%

The preparation of the solid polished wafers of tuff was described in detail by Knauss and Beiriger (1984a). After a thorough ultrasonic washing, representative unreacted wafers of tuff are observed by an SEM that shows their surfaces to be largely devoid of the adhering ultrasonic material or polishing compound (alumina) that might be expected to result from the cutting and grinding operations.

Wafers prepared from outcrop tuff were used in two experiments (DB6 and DB7). The outcrop tuff (Tpt FR) was characterized in the same manner as the drillcore tuff; the results were presented by Knauss (1984) and Knauss et al. (1985). In general, the mineralogy, bulk composition, and composition of the individual mineral phases of drillcore and outcrop tuff are similar. They differ primarily in devitrification texture, which may be used to infer a higher relative stratigraphic position for the outcrop sample within the Tpt section (Byers, 1984).

The compositions of the phenocryst phases and the matrix (a mixture of finely crystalline quartz and/or cristobalite and alkali feldspar) of the G-1 1232 drillcore sample were determined using quantitative WDS analysis done by electron microprobe. The analytical conditions used were described in some detail by Knauss (1984). Both a polished thin section and a polished core wafer were analyzed, and the results are generally in good agreement. Some heterogeneity has been observed, however, in the phase geochemistry. We attribute this heterogeneity to a number of factors related to sampling error and do not consider it as sufficient evidence in itself for differences in original magma composition. In fact, we

have evidence to the contrary. Thirty analyses taken from potential repository depth in holes USW G-1, USW GU-3, and USW G-4 and from outcrop on Iran Ridge and Busted Butte (Knauss, 1985; Schuraytz, 1985) are very similar. Although the Tpt ashflow sheet is chemically zoned within the phenocryst-poor rhyolitic interval in which the potential repository level is located, the chemical variation is minor. Hence, we would expect bulk mineral compositional variation to have little or no influence on the experimental results. Because of the sporadic occurrence of large phenocrysts (Byers, 1984), the microprobe data from individual phases may tend to reflect the presence or type of zoning in phenocrysts from each sample. Ideally, a large number of samples (thin sections or wafers) should be analyzed to characterize the phenocryst geochemistry more extensively; this would allow differences between drillcore and outcrop samples, if they exist, to be documented accurately.

Phenocrysts analyzed include plagioclase, alkali feldspar, biotite, quartz, and magnetite. Also included are WDS analyses of matrix and an EDS semiquantitative analysis of manganese-rich fracture-filling material. These data are presented in Appendix A for the thin section (Table A1) and the polished wafer (Table A2).

Ternary diagrams of feldspar compositions have been constructed to illustrate the dominant composition and compositional range for the primary mineral phases present as phenocrysts in the drillcore samples.

Plagioclase feldspar compositions from the core wafer and thin section are plotted in Fig. 1. Plagioclase ranges from An_{13} to An_{36} (An = anorthite) in the core wafer, with the maximum occurring at approximately An_{17-18}. In the thin section, plagioclase exhibits a wider variation from An_{5} to An_{50}. Compositions of less than 12 mole% An are usually analyses of the edges of phenocrysts, which tend to be more sodic; values in the range from 40 to 50 mole% An are usually from the cores of phenocrysts. While this small population suggests that plagioclase feldspars from the core wafer could be about 3 to 4 mole% richer in the An component on the basis of median values, significantly more analyses are required to establish this difference and to distinguish the effects of zoning within individual phenocrysts.

Potassium feldspar (K-feldspar) compositions from the core wafer and thin section are also plotted in Fig. 1. The K-feldspar in the core wafer varies between Or_{53} and Or_{63} (Or = orthoclase), with the maximum lying near Or_{62}. In the thin section, the K-feldspar ranges from Or_{35} to Or_{52}, with the maximum occurring at Or_{45}. If the K-feldspar compositions of the core wafer and thin section are considered separately, the K-feldspar from the core wafer is clearly richer in the Or component. If they are considered part of the same population, the K-feldspar distribution is distinctly bimodal and resembles the Or distribution observed in the outcrop sample Tpt FR (Knauss, 1984). Again, more analyses are needed to clarify this point.

Biotite is the most common mafic phase in the Topopah Spring tuff. Although the biotite was badly altered, we were able to obtain a few reliable analyses from the thin section. To indicate biotite purity, we have employed the results of Engels' (1972) exhaustive study of 2700 biotites, which concluded that biotites "showing less than 8% K_2O are likely to be contaminated . . ." The ratio $(FeO/FeO + MgO + MnO) \times 100$ of the analyzed biotites with K_2O greater than 8% ranges from 67 to 73.

Histograms of compositional data for the plagioclase feldspar, K-feldspar, and biotite determined in polished wafers and thin sections of the outcrop material Tpt FR were reported previously by Knauss (1984). The results may be summarized as follows. The plagioclase varies from An_{12} to An_{43}, with a prominent maximum composition occurring near An_{17}. Potassium feldspar ranges from Or_{52} to Or_{63}, with a maximum lying about Or_{56}. The analyzed ratio $(FeO/FeO + MgO +$

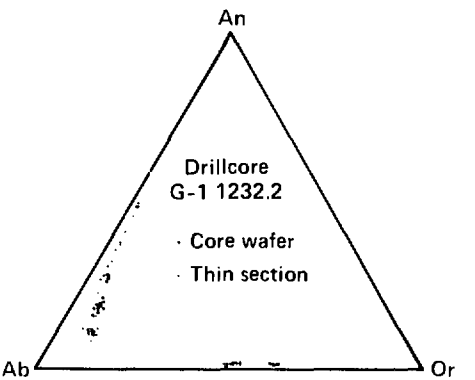

Figure 1. Composition (mole%) of coexisting feldspars from the core wafer and thin sections of drillcore specimen USW G-1 1232 plotted in the ternary albite (Ab)-anorthite (An)-orthoclase (Or).

MnO) × 100 in biotite from the outcrop samples ranges from 47 to 71, with two populations—one with values clustering around 48 and the main population centered on 62.

In general, the compositions of the primary mineral phases present in the two samples—one from drillcore and one from outcrop—are similar.

Experimental Techniques

All experiments were carried out in Dickson-type, gold-bag rocking autoclaves. These vessels have an inner, flexible gold bag (containing the reacting solids and fluid) that collapses as sample fluid is withdrawn. To maintain constant pressure, additional distilled water is injected into the surrounding autoclave (Seyfreid et al., 1979). The gold bag has a volume of approximately 230 ml; thus, many samples may be taken from the same solution without quenching the run. The gold bag is sealed by a titanium collar and titanium head containing a gold filter, which prevents solids from being removed when a fluid sample is withdrawn. The fluid sample passes through a gold capillary tube contained within a stainless steel exit tube, flows past a titanium needle-valve assembly, and is bled through a Teflon nipple into a plastic syringe. In this way, the solution is exposed to gold and titanium only during the experiment and to Teflon and plastic upon sampling.

The entire pressure vessel is contained within a large furnace that is heated by an electrical resistance heater. The whole assembly (pressure vessel plus furnace) is rocked constantly through 180°C, at a rate of six cycles per minute, on a large rack that holds two furnaces. The autoclave is pressurized with distilled water, and the pressure is monitored with gauges mounted on each furnace. The furnace temperature is controlled by digital proportionating temperature controllers and is monitored throughout the course of the experiment. Chromel-alumel thermocouples and digital thermometers accurate to ±1°C are used to measure internal vessel temperature. The advantages of this type of system over the more common cold-seal vessels used for rock-water interaction experiments have been described previously (Walther and Orville, 1983; Knauss et al., 1985).

The titanium head in the reaction cell has been modified slightly to hold the solid polished wafers run in these experiments. The titanium gland nut that holds the gold filter has been threaded to accept a small titanium bolt. The polished wafer, which has a small hole drilled in its center, is sandwiched between two washers cut from gold mesh, and the titanium bolt is used to suspend the wafer beneath the titanium head of the reaction cell. In this way, the wafer is exposed to the solution and affords a convenient surface upon which secondary minerals from the hydrothermal interaction may grow.

The experiments reported herein ranged from 49 to 66 days in duration. Longer-term runs, described earlier (Knauss et al., 1987), have lasted up to 303 days. Unlike the crushed tuff experiments, during which the rocking motion is halted only while sampling (Knauss et al., 1985), the wafer experiments are rocked only a few hours each day. This periodic rocking was a compromise between the two extremes: the continuous rocking required to maintain complete solution-solid contact in experiments with crushed tuff, and the no-rocking permitted in experiments with solid monoliths suspended so as to maintain solution-solid contact. If the wafer were to break during the run and fall to the bottom of the gold bag, this periodic rocking would maintain solution-solid contact while mitigating the destructive effects of continuous rocking on the electrical components of the rack.

Fluid samples are drawn from the gold bag, through the titanium valve, and injected into a preweighed disposable syringe. First, however, 1 ml of fluid is drawn off and discarded to bleed any stagnant solution from the gold capillary tube. Aliquots of fluid are drawn slowly to avoid flashing and are used for the analyses described in more detail below. Pressure is maintained with a Sprague pump during the sampling procedure. For the short-term experiments, an effort is made to sample the progression 1, 2, 4, 8, 16, 32, 48, and 64 days after starting. At the conclusion of each run, the furnace power is switched off, and the pressure vessel is disassembled as soon as practical (after approximately 10 to 15 hours, depending on run temperature).

The fluid samples are used for a variety of analyses:

- An unfiltered sample is used for an immediate pH measurement, using a glass electrode and a digital meter.

- A filtered (0.1-μ) and acidified (Ultrex nitric acid) sample is run both full-strength and diluted for cation analysis, using inductively coupled plasma-emission spectrometry (ICP-ES).
- A filtered, acidified sample is run full-strength for potassium, using atomic absorption (AA).
- A filtered sample is used for anion analysis, using ion chromatography (IC).

For the earlier experiments reported herein, carbonate alkalinity was measured on unfiltered samples using IC only. Although efforts were made to prevent gas exchange (storage in glass vials and analysis the same day in most cases), some analyses showed evidence of volatile gain or loss (pH or alkalinity change). The alkalinity data in this report have been edited to point out analyses that are known to be suspect because of gross changes in solution pH between sampling and alkalinity analysis or abnormally high measured alkalinity values. In addition, attempts to model the results using EQ3/6 (Delaney, 1985) show a systematic negative charge balance in many experiments, even for analyses not edited using these criteria. Charge balancing on alkalinity was found to result in reasonable and consistent values for each experiment, again arguing for a problem in the IC alkalinity data. In later experiments, the total CO_2 was determined by total inorganic carbon analysis with infrared (IR) detection of the evolved CO_2 gas. These IR CO_2 measurements were made immediately upon sampling, by direct injection of unfiltered aliquots of fluid from the sampling syringe. The precision and accuracy of this sampling procedure (*vis a vis* flashing of dissolved gas) and analytical technique were investigated by running standard sodium carbonate solutions in the Dickson-type autoclaves at 90 and 250°C. Repeated measurements demonstrate that these immediate IR CO_2 analyses are far superior to those done either by spectrophotometric titration or by IC on fluid provided for analyses at some time (even only a few hours) following sampling.

At the completion of each run, the solid polished wafers are removed from the titanium and gold reaction cells and rinsed gently in distilled water. The wafers are then air-dried in a desiccator to constant weight.

The primary analytical tool for post-test solid phase analysis was the SEM/EMP. The approach was outlined in a previous report (Knauss and Beiriger, 1984a). Basically, it involved a low-magnification scan of the entire wafer to locate phenocrysts and matrix areas for subsequent WDS analyses and a high-magnification scan of the entire wafer to locate run products growing on the surface of the wafer. The analytical conditions for the post-run WDS analyses of phenocrysts and matrix were identical to those used in the pretest analyses (Knauss, 1984). In most cases, the secondary minerals found were characterized compositionally using EDS only. The EDS spectra were plotted, and a semiquantitative analysis was performed on the basis of these spectra. In two experiments (DB7 and DB9), however, the zeolite (dachiardite) crystals formed were so large (up to 70 μ in the long dimension) that they could be removed easily from the surface of the wafer by handpicking under a binocular microscope. These zeolites were analyzed by XRD, using a Gandolfi camera to yield precise cell dimensions, and a polished grain mount was prepared for WDS analysis. Details concerning the analytical conditions used to obtain 45 quantitative (alkali-aluminum balance, $(E) < \pm 7\%$; Passaglia, 1970) WDS analyses are contained in Appendix D.

Analytical Results

Because of the large amount of analytical data, only plots summarizing the evolution of fluid composition with time will be presented within the body of this report. Complete tables of fluid composition data can be found in Appendix B. Similarly, only ternary diagrams summarizing the post-test EMP analyses will be presented within the body of the report. Complete tables of reacted-tuff primary mineral-phase compositional data appear in Appendix C. As mentioned previously, Appendix D describes in detail the characterization work done to define precisely the chemical composition (using quantitative EMP/WDS analyses), cell constants (using precise Gandolfi XRD camera measurements), and crystal habit (using SEM observations) of the dominant zeolite mineral (dachiardite) produced in abundance in the 250°C experiments. Appendix E is a detailed description of the characterization work done on secondary minerals; this work entailed using EDS

spectra to determine what elements were present and semiquantitative analyses based on these spectra to determine their approximate composition.

J-13 Water Alone Heated at 150 and 90°C

Although J-13 water is a relatively dilute natural ground water, it does contain dissolved constituents, and its composition can be affected by heating alone. To determine which changes in J-13 water composition were due to hydrothermal interaction between the rock and water and which were due to heat alone, we conducted two experimental runs without tuff. These runs were made at 150°C (DB19) and 90°C (DB18), at 50-bar pressure, and lasted 52 days.

Figure 2 shows the chemical evolution of J-13 water heated at 150°C for 52 days (DB19). Complete cation and anion analyses and pH for all samples taken are given in Table B1. Note that the aluminum concentration for Day 0 is much higher than that for typical J-13 analyses. A tenfold dilution of the same sample yielded an aluminum concentration at detection limit (0.028 ppm), suggesting a true aluminum concentration of less than 0.28 ppm. Also, analytical problems precluded making any potassium analyses on the full-strength samples from Day 0 to Day 8 inclusive. Thus, only the tenfold-diluted sample was available, and the analyses are much less precise. The analysis shown as Day 53 is actually a sample of quenched fluid taken from the gold bag immediately upon disassembly of the autoclave.

The effect of heat on J-13 water alone is seen primarily in two processes: the alkaline earths (calcium and magnesium) are inferred to precipitate as carbonates because of their retrograde solubility, and the pH and alkalinity decrease. Despite a minor dip in silicon during the run, there is no apparent decrease in silicon or any other dissolved constituent by the end of the run. The quench sample taken at the end of the run shows, upon cooling, that the magnesium remains low, but the fluid gains back calcium as the carbonate redissolves. The pH adjusts accordingly. The calcium concentration in the full-strength quench (Day 53) sample is actually higher than the starting J-13 water concentration, which suggests an analytical problem. A tenfold dilution of this sample results in a concentration of 11.7 ppm calcium, hence the conclusion that calcium is released back into solution upon cooling. The other dissolved species remain unchanged upon quenching.

Plots of the results of heating J-13 water to 90°C for 52 days (DB18) are given in Fig. 3, and the complete set of chemical analyses is given in Table B2. Note that the aluminum concentration in this Day 0 sample is again much higher than that found in typical analyses of J-13 water; however, tenfold dilution confirms the aluminum concentration in this sample. Although the Day 0 samples for experiments DB18 and DB19 were pulled from the same bottle of J-13 water at the same time, higher than normal (full-strength vs diluted) aluminum concentration was confirmed in only one of the samples. We consider this difference in aluminum concentration to be an analytical problem (or contamination by the analyst) rather than evidence of contamination of the J-13 water used in the experiments. The problems with the potassium analyses mentioned previously were also present in experiment DB18. The effects of heating this water to 90°C were very minor. The calcium concentration decreased slightly during the first few days, but the changes were minor and just outside analytical error. The magnesium concentration appeared to be significantly lower in the Day 16 and Day 32 samples but rose in the quench sample. The pH and all other constituents were basically unchanged.

Because no tuff was present in experiments DB18 and DB19, there are no post-test analyses of reacted tuff. No evidence of secondary mineral precipitation was evident within the gold bag or on the titanium head of the reaction cell. This is not inconsistent with the inference of carbonate precipitation from the fluid analyses. Since the calcium redissolved upon quenching, we can assume that magnesium was the only remaining carbonate. The total amount of magnesium removed from solution would produce about 1 mg of carbonate, which would be difficult to detect if it were dispersed as a fine particulate either in suspension in the fluid or adhering to the gold bag or titanium head.

Tpt G-1 1232 (DB9) and Tpt FR (DB7) Plus J-13 Water Heated to 250°C

Drillcore sample Tpt G-1 1232 was reacted with J-13 water at 250°C and 50 bar for 66 days in experiment DB9. The composition of the fluid phase, plotted as a function of time, is given in Figs. 4 and 5. The complete cation and anion analyses are given in Table B3. A quench sample was not taken at the termination of the run.

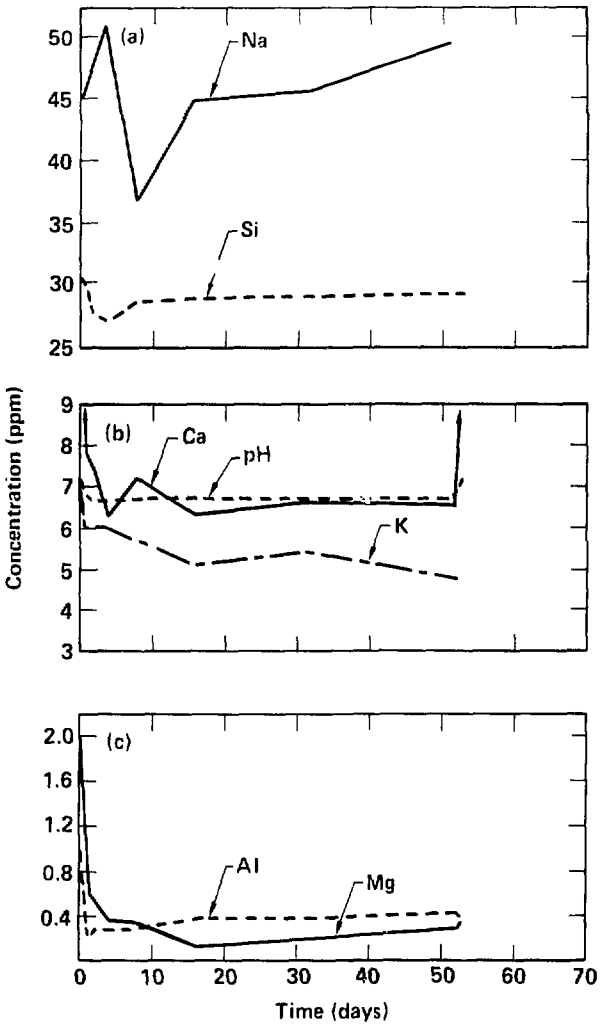

Figure 2. Fluid composition vs time for J-13 water heated alone at 150°C in experiment DB19. (a) Sodium and silicon; (b) calcium, potassium, and pH; (c) aluminum and magnesium. The initial (12.6 ppm) and final (11.7 ppm) calcium concentrations are not plotted.

The hydrothermal reaction of tuff at 250°C resulted in significant changes in J-13 water chemistry. The solution analyses show that silicon increased quickly to near cristobalite saturation (345 ppm), reaching steady state in two weeks. Aluminum increased rapidly at first, then decreased more slowly than it increased (suggesting kinetically inhibited precipitation), only to rise again somewhat in the last sample taken. Calcium was removed to low levels, and magnesium was

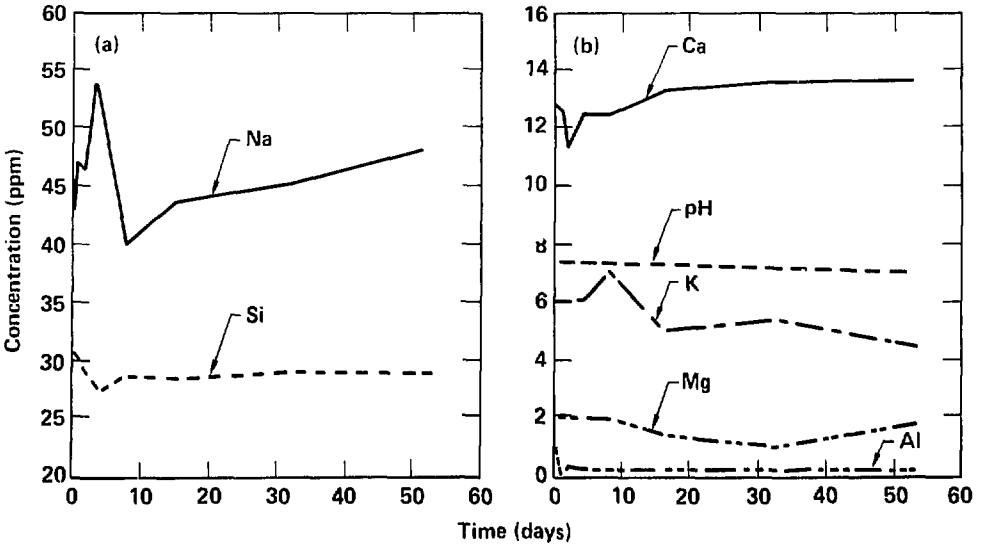

Figure 3. Fluid composition vs time for J-13 water heated alone at 90°C in experiment DB18. (a) Sodium and silicon; (b) calcium, potassium, aluminum, magnesium, and pH.

almost completely removed. The pH dropped quickly and then remained constant. The *in situ* pH calculated using EQ3NR was distinctly basic (pH 7.2), inasmuch as neutral pH at 250°C is about pH 5.5. Although there was no clear trend in the evolution of potassium concentration with time, all samples collected over the first 32 days had a potassium concentration that was higher than the initial J-13 value, while the final sample collected after 66 days of interaction had a slightly lower potassium concentration. The sodium concentration was essentially unchanged. Following an initial decrease in alkalinity, the anions remained essentially unchanged.

The effects of the hydrothermal alteration of tuff at 250°C were readily apparent in the SEM observation. The effects on phenocrysts were seen as highlighting of twinning by the formation of etch pits on feldspars (Holdren and Berner, 1979) and the general corrosion of biotite. The smaller alkali feldspar crystals formed by granophyric devitrification of the tuff matrix and by vapor phase deposition in lithophysal cavities and voids appeared to be particularly prone to attack, as did the other fine-grained devitrification products that comprised the matrix (Appendix E).

The post-test compositions of the plagioclase feldspar and K-feldspar in experiment DB9 are plotted on an Ab-Or-An (Ab = albite) ternary diagram in Fig. 6. The complete EMP/WDS analyses are provided in Table C1. The plagioclase feldspar varied from An_1 to An_{42}, with the dominant composition occurring between $An_{16\text{-}18}$ mole%. The composition of the potassium feldspar was found to range from Or_{40} to Or_{73}, with a median in the vicinity of $Or_{56\text{-}61}$ mole%. None of the biotite phenocrysts was amenable to WDS analyses following reaction, having been altered too badly by reaction with the fluid. The total wafer weight loss was 0.1319 g, or 5.67% of the original wafer weight.

The hydrothermal alteration at 250°C produced several identifiable secondary minerals. Other run products may only be inferred on the basis of their chemical composition, estimated from EDS spectra and from crystal habit or morphology seen in SEM photographs.

The dominant secondary mineral produced was the relatively rare dachiardite (Knauss and Beiriger, 1984b), which occurred as abundant, large prismatic crystals with smaller interpenetrating crystals and rosettes of crystals. Because the

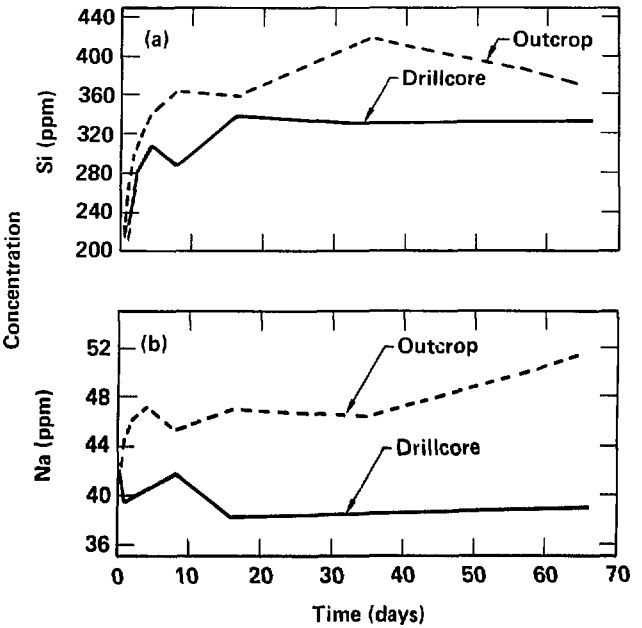

Figure 4. Fluid composition vs time for J-13 water reacted with a solid polished wafer of drillcore sample Tpt G-1 1232 and a solid polished wafer of outcrop sample Tpt FR at 250°C in experiments DB9 and DB7. (a) Silicon; (b) sodium. Initial silicon concentrations (D = 29.1 ppm; O = 29.2 ppm) are not plotted.

dachiardite was so common and occurred in such large clusters of crystals, it could be thoroughly characterized by hand-picking from the surface of the wafer once the experiment was completed. This detailed characterization and analysis form the basis for Appendix D, which details how the dachiardite was positively identified on the basis of its XRD pattern produced in a Gandolfi x-ray camera. By this method, some 26 lines were matched with those contained on JCPDS Card 18-467 for Elba dachiardite. The measured d-spacings of lines were then used in a linear regression technique to calculate cell constants. The refined cell constants were:

a_o = 18.645 Å
b_o = 7.483 Å
c_o = 10.247 Å
V_o = 1358 Å^3
β_o = 108°09′

A polished grain mount of dachiardite crystals was analyzed by WDS. On the basis of 45 analyses [all with alkali-aluminum balance (E) $< \pm 7\%$; Passaglia, 1970], with water calculated by difference, the composition was

$$Ca_{2.10}K_{0.34}Na_{0.16}[Al_{4.87}Si_{19.15}Or_{48}]\cdot 13.9\ H_2O,$$

and the calculated density was 2.18 g/cm^3. There was an inverse relation between silicon/aluminum and calcium and possibly a weak direct relation between silicon/aluminum and potassium, which suggests some degree of substitution of Na + K + Si for Ca + Al. Step-scan WDS analyses every 2 μ across and along the dachiardite grains showed no evidence of zoning for sodium, potassium, or calcium.

Other secondary minerals inferred to be present were mordenite (high confidence), a minor amount of a poorly crystalline, potassium-bearing

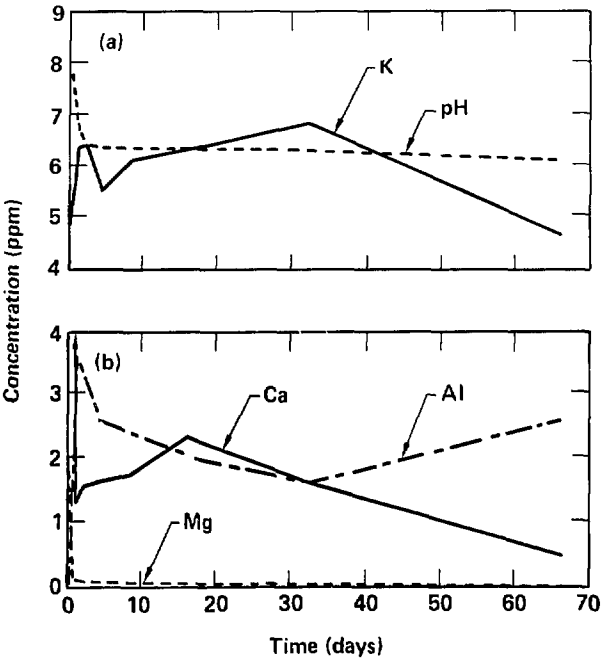

Figure 5. Fluid composition vs time for J-13 water reacted with a solid polished wafer of drillcore sample Tpt G-1 1232 at 250°C in experiment DB9. (a) pH and potassium; (b) aluminum, calcium, and magnesium. The initial calcium concentration (13.1 ppm) is not plotted.

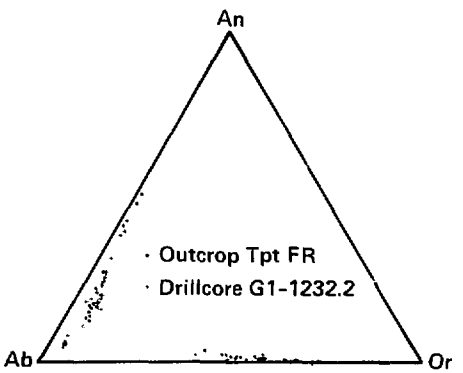

Figure 6. Composition (mole%) of coexisting feldspars following experiments DB7 (outcrop) and DB9 (drillcore) plotted in the ternary albite (Ab)-anorthite (An)-orthoclase (Or).

claylike phase (lower confidence), and, very rarely, a pure silicon phase (possibly cristobalite). SEM photographs of these secondary minerals, EDS spectra, and semiquantitative analyses based on them are contained in Appendix E. Dachiardite and mordenite were far more abundant than any of the other secondary phases. We cannot exclude the possibility that the minor amount of claylike material observed resulted from quenching the vessel at the end of the run (Appendix D).

The other polished wafer experiment run at 250°C (DB7) used outcrop tuff. The fluid-phase results from this experiment are plotted in Figs. 4 and 7, and the complete analyses are given in Table B4. The trends in fluid compositio for the drillcore and outcrop experiments were very similar, although the absolute values differ because of the effects of evaporative salts that remained in the outcrop wafers despite the large amount of water used in the cutting and polishing operations

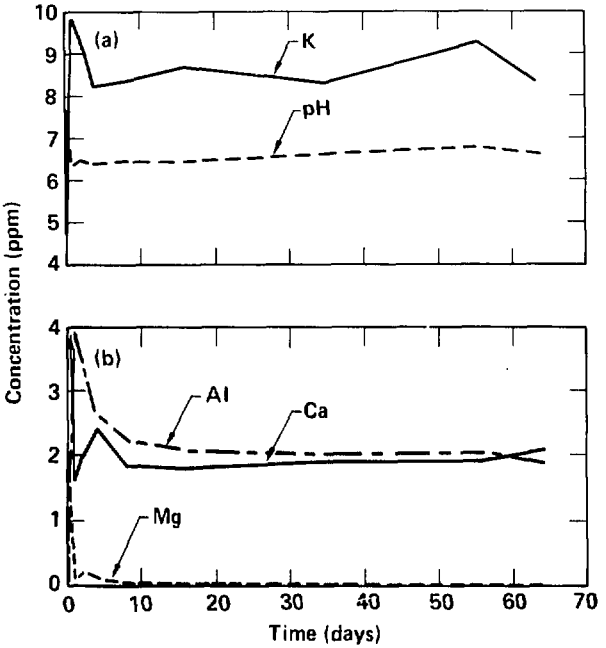

Figure 7. Fluid composition vs time for J-13 water reacted with a solid polished wafer of outcrop sample Tpt FR at 250°C in experiment DB7. (a) Potassium and pH; (b) aluminum, calcium, and magnesium. The initial calcium concentration (13.1 ppm) is not plotted.

(Oversby and Knauss, 1983). The effect of evaporites (relative to the initial J-13 water composition) was most noticeable in the elevated concentrations of potassium (increased 77%) and sodium (increased 25%). The alkalinity and pH were somewhat higher in the outcrop experiment. The silicon concentration was also higher in the outcrop experiment than it was in the drillcore experiment, although it exceeded cristobalite solubility by only 8% at the end of the run. The behavior of calcium and magnesium was similar in both experiments.

Post-test analyses of mineral phases within the outcrop wafer showed results similar to those seen for the drillcore experiment at 250°C. The compositions of the coexisting ternary feldspars are plotted in Fig. 6, and complete EMP/WDS analyses are provided in Table C2. The plagioclase feldspar in experiment DB7 varied from An_{10} to An_{52}, with a median occurring at An_{16}. The composition of the K-feldspar was found to range from Or_{41} to Or_{92}, with a median at approximately Or_{56} mole%. The ratio (FeO/FeO + MgO + MnO) × 100 of analyzed biotites varied from 58 to 68. Total wafer weight loss was 0.1344 g, or 5.67% of the original wafer weight.

The dominant secondary mineral in the outcrop experiment was again the zeolite dachiardite. Its composition was identical to that produced in the drillcore experiment. Considering that the composition of the starting materials was essentially identical in both experiments (drillcore Tpt vs outcrop Tpt), the only differences being that a small amount of evaporite minerals was present in the outcrop sample and that the fluid compositions produced in each experiment were very similar, it is not surprising that the run products and their compositions were identical. In fact, the previously determined composition for dachiardite was a combination of analyses from each experiment. To

illustrate, we consider the results from each experiment separately in Appendix D and demonstrate that drillcore and outcrop dachiardite are identical within very tight error limits. Other run products inferred to be present on the wafer were also similar: a potassium-bearing, claylike phase and very rare cristobalite. Also present, however, were a few small, highly corroded rhombs of calcite, which contained significant amounts of silicon as well. These few crystals were all less than 10 μ in the longest dimension and, from their appearance, were actively dissolving. SEM photographs, EDS spectra, and semiquantitative analyses based on them are given in Appendix E for experiment DB7. Mordenite was notably absent from the outcrop wafer.

Tpt G-1 1232 (DB8) and Tpt FR (DB6) Plus J-13 Water Heated to 150°C

We ran two experiments at 150°C, using polished wafers of drillcore tuff and outcrop tuff. The results of the experiment run with Tpt G-1 1232 drillcore tuff are shown in Figs. 8 and 9. Complete aqueous phase analyses are given in Table B5. As it had at 250°C, the silicon concentration rose exponentially to a value equivalent to cristobalite saturation (122 ppm) by the end of the run. However, the rate at which this value was approached was considerably slower. Similarly, the aluminum rose to a maximum at Day 4 and then decreased to a constant value. The potassium also behaved in a similar manner, taking until Day 16 to reach a maximum before steadily decreasing. Sodium rose slowly during the course of the run. Calcium decreased quickly, but not to the low levels reached at 250°C, and magnesium was removed to low levels. Correspondingly, the pH dropped, as did the alkalinity, and then remained relatively constant. With the exception of a spuriously high Cl concentration at Day 8, the anions remained unchanged. The more complex behavior of calcium, potassium, and aluminum, as at 250°C, reflects the competing effects caused by the dissolution and reactants and the sometimes kinetically inhibited precipitation of metastable run products.

We investigated the effects of hydrothermal alteration on the primary minerals by analyzing the composition of plagioclase and the coexisting K-feldspar and biotite. The results of the feldspar analyses are presented in Fig. 10. Complete analyses as oxides are presented in Table C3. In

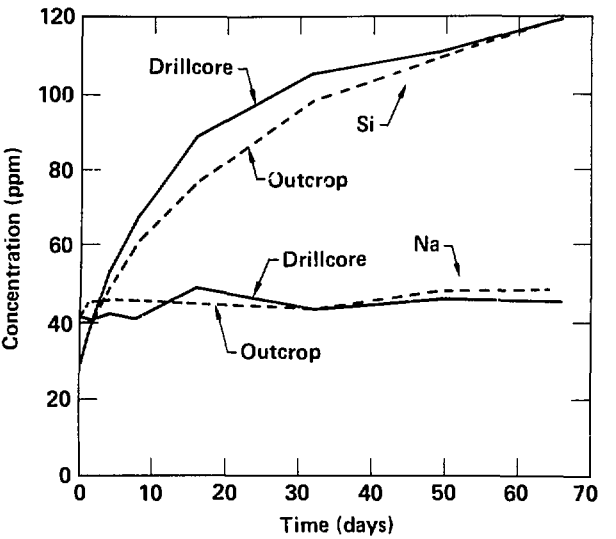

Figure 8. Fluid composition vs time for J-13 water reacted with a solid polished wafer of drillcore sample Tpt G-1 1232 at 150°C in experiment DB8 and with a solid polished wafer of outcrop sample Tpt FR at 150°C in experiment DB6.

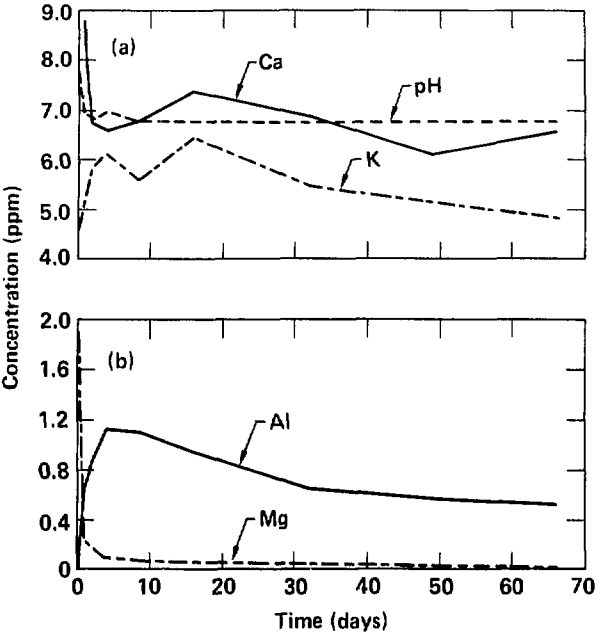

Figure 9. Fluid composition vs time for J-13 water reacted with a solid polished wafer of drillcore sample Tpt G-1 1232 at 150°C in experiment DB8. (a) Calcium, pH, and potassium; (b) aluminum and magnesium.

experiment DB8, the plagioclase varied from An_{11} to An_{27}, with the main peak occurring at An_{18} mole%. The composition of the K-feldspar ranged from Or_{43} to Or_{66} mole%. No clear maximum was delineated in the K-feldspar composition, but a continuum of compositions occurred in the range Or_{53} to Or_{64}. Only five biotites were analyzed successfully in experiment DB8. The ratio (FeO/FeO + MgO + MgO) × 100 was found to vary from 46 to 67. Total wafer weight loss was 0.0411 g, or 1.83% of the initial wafer weight.

The secondary minerals produced by the hydrothermal alteration of the tuff at 150°C were less developed, less crystalline, and far less abundant than those at 250°C. Because none of them was larger than about 10 μ, the detailed characterization done with the zeolite produced at 250°C could not be repeated here. Thus, the identity of the run products may only be inferred from their EDS spectra and morphology. Although the total amount of run products is very small, they are thought to include potassium-, calcium-, magnesium-, and/or iron-bearing claylike phases, gibbsite (or boehmite), and cristobalite. Examples of these phases are given in Appendix E.

The 150°C experiment conducted with outcrop tuff (DB6) resulted in an evolving fluid phase whose composition is represented in Figs. 8 and 11. Complete analyses are given in Table B6. The trends seen at 150°C in the drillcore experiment can also be seen in the DB6 experiment with outcrop tuff. Again, the silicon rose exponentially to essentially cristobalite saturation. By Day 8, the aluminum had risen to a maximum that was only slightly higher than the maximum in the drillcore experiment and then decreased to comparable levels. The sodium and magnesium also behaved as they had in the drillcore experiment: the magnesium was quickly removed from solution, and the sodium rose slowly. There were slight differences, however, in alkalinity (Cl, NO_3^-, and SO_4^{-2}), with the outcrop values being higher than

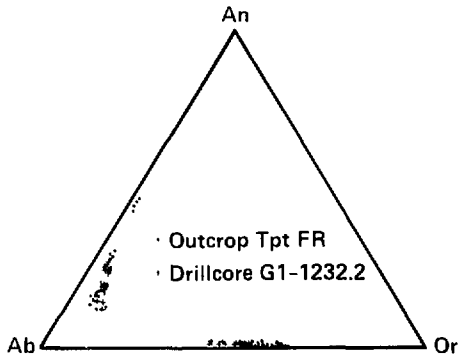

Figure 10. Composition (mole%) of coexisting feldspars following experiments DB6 (outcrop) and DB8 (drillcore) plotted in the ternary albite (Ab)-anorthite (An)-orthoclase (Or).

those in the drillcore experiment. The most notable differences, however, were in potassium and calcium. The potassium rose to and remained at a higher concentration in the outcrop than it had in the drillcore experiment. The calcium decreased initially as it had in the drillcore experiment, but not to as low a concentration, and then rose as the experiment progressed. As the description of the secondary minerals reveals, this is in agreement with the observation of run products.

The post-test analyses of primary phases are summarized in Fig. 10, which is a ternary diagram of the coexisting feldspars. The complete analyses on which these calculated compositions are based are given in Table C4. In experiment DB6, the plagioclase feldspar varied from An_{11} to An_{37}, with the most frequent composition occurring at An_{16-18} mole%. The alkali feldspar ranged in composition from Or_{52} to Or_{64}. No central maximum was seen in the K-feldspar composition, just the

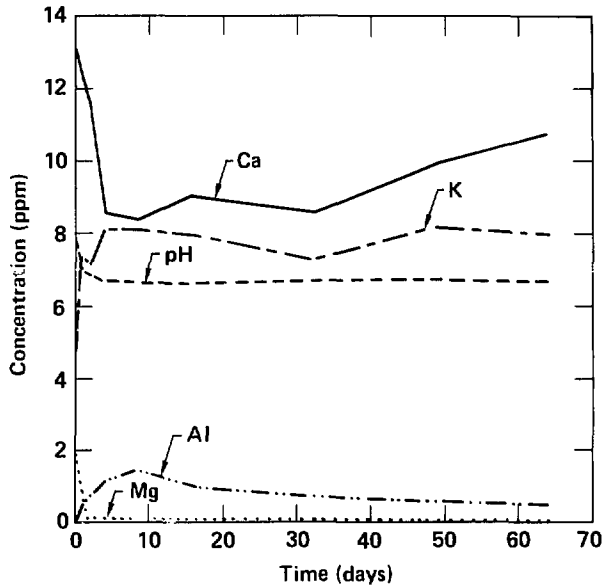

Figure 11. Fluid composition vs time for J-13 water reacted with a solid polished wafer of outcrop sample Tpt FR at 150°C in experiment DB6. (a) Calcium, pH, and potassium; (b) aluminum and magnesium.

continuum mentioned above. The (FeO/FeO + MgO + MnO) × 100 ratio of analyzed biotites was found to vary from 47 to 69. At the termination of experiment DB6, the wafer had lost 0.0363 g, or 1.54% of its initial weight, as a result of its reaction with the J-13 water.

One difference between the run products formed in the 250°C drillcore experiments and those formed in the 250°C outcrop experiments was the presence of small, severely corroded, silicon-rich calcite rhombs in the outcrop runs. At 150°C, the secondary minerals formed using either drillcore or outcrop tuff were again very similar, primarily potassium-, calcium-, magnesium-, and iron-bearing claylike run products that were very small and poorly crystalline. Again, the only difference was the presence of calcite as a run product in the outcrop experiment. This time, however, the calcite rhombs were much larger than those at 250°C, not as severely corroded, and contained only minor amounts of occluded silicon. Good examples of the composition of these run products, based on EDS spectra and SEM photographs, are shown in Appendix E.

Tpt G-1 1232 Plus J-13 Water Heated to 90°C (DB14)

The only experiment (DB14) run at 90°C used a polished wafer of drillcore tuff. The composition of the aqueous phase during experiment DB14 is shown in Fig. 12. The complete fluid analyses are given in Table B7. At this low temperature, with the diminished surface area offered by the polished wafer (as compared with crushed material), the extent of the reaction between the J-13 water and tuff was very small. The silicon data were somewhat scattered, and there was only a minor increase in silicon concentration by the end of the run. The solubility of alpha-cristobalite at 90°C was about 49 ppm; hence, saturation was clearly not reached during this run. The sodium and calcium remained unchanged, but there was a small decrease in the magnesium concentration. This decrease in magnesium was coincident with a small decrease in pH that occurred throughout the experiment. Aluminum was only determined in the last three samples taken during the experiment, suggesting that it may increase slightly with time. The anions were essentially constant, but the alkalinity data were of such poor quality that little can be said about the variation in alkalinity through the course of the experiment.

We determined the compositions of the primary phases of plagioclase, alkali feldspar, coexisting feldspar, and biotite; the feldspar data are plotted in Fig. 13. The oxide analyses on which these data are based are presented in Table C5. The table also includes some EMP analyses of an

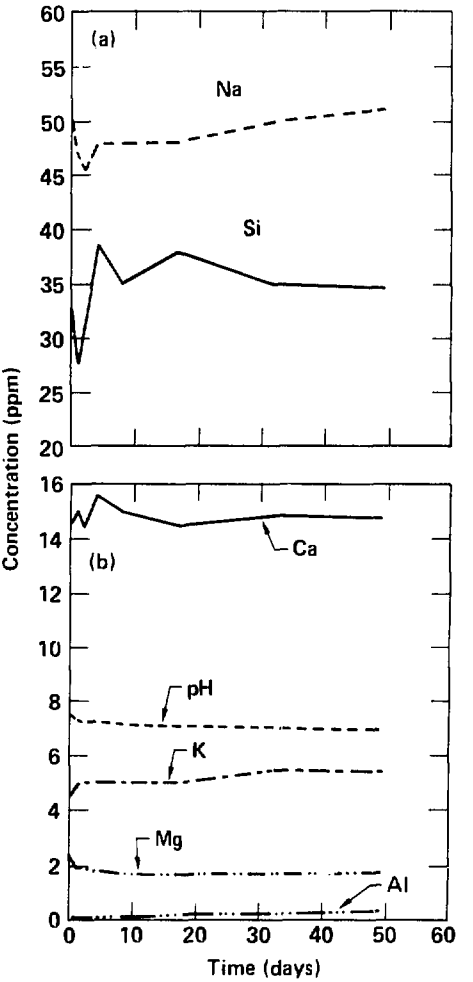

Figure 12. Fluid composition vs time for J-13 water reacted with a solid polished wafer of drillcore sample Tpt G-1 1232 at 90° in experiment DB14. (a) Sodium and silicon; (b) aluminum, calcium, potassium, magnesium, and pH.

unknown complex manganese-aluminum oxide with anomalously low totals because of the calculation of manganese as MnO, rather than as a more oxidized form. The plagioclase in experiment DB14 varied from An_{12} to An_{31}, with the dominant composition being An_{17-18} mole%. The composition of the alkali feldspar was found to range from Or_{46} to Or_{64} mole%. No clear maximum was defined by the data within this interval. Only four biotites could be analyzed successfully from this experiment, and the ratio (FeO/FeO + MgO + MnO) × 100 varied from 37 to 58. The wafer lost only 0.0029 g, or 0.10% of its initial weight. This is concordant with the small degree of dissolution inferred from the changes in water composition with reaction time at 90°C.

Despite exhaustive efforts, no run products could be located on the surface of the reacted core wafer. Whereas there was good evidence of dissolution of the primary phases at 150 and 250°C, such as etch pits on the feldspar phenocrysts, at 90°C the reacted wafer looked essentially identical to the unreacted wafer, Tpt G-1 CWO_d, which was used as a control.

Tpt G-1 1232 Plus Distilled Water Heated to 150°C (DB16) and 90°C (DB17)

The NNWSI project has adopted water from well J-13 as a reference ground water composition

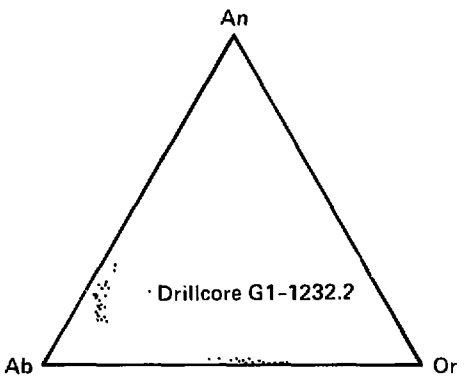

Figure 13. Composition (mole%) of coexisting feldspars following experiment DB14 (drillcore) plotted in the ternary albite (Ab)-anorthite (An)-orthoclase (Or).

for waste package and other experimental work; however, the exact composition of water in the unsaturated zone is unknown. To examine what effects the starting composition of the fluid phase had on the reacted water composition in these tuff-water interaction experiments, we ran two experiments using distilled water as the reactor fluid. In both of these experiments, polished wafers of drillcore tuff, Tpt G-1 1232, were used as the solid phase.

The distilled water experiment run at 150°C (DB16) resulted in the evolving fluid depicted in Figs. 14 and 15. The complete fluid analyses are presented in Table B8. Despite the fact that it initially contained no dissolved silicon, the distilled water gained enough silicon in one week to achieve a concentration roughly equal to that in the corresponding experiment with J-13 water (DB8). By the end of the run, the formerly distilled water may have contained slightly more dissolved silicon (13%) than was present in the J-13 water. It may also have gained an absolute amount of sodium roughly similar to that gained by the J-13 water in the DB8 experiment, even though its relative increase in sodium was much larger. The solution pH in the distilled water experiment rose slowly throughout the experiment and eventually exceeded that in the DB8 experiment. The buffer capacity was low because of the absence of carbonate; thus, hydrolysis of the feldspars and other silicates produced a rise in pH. The alkalinity increased during the course of the experiment, but was still less than half that in the corresponding J-13 experiment. Both calcium and magnesium started out much lower in the distilled water experiment, but their behavior was similar to that seen in experiment DB8. The dissolved potassium in the two experiments was also similar in that the concentration rose initially and then declined. The anion content was as low to undetectable throughout the experiment.

Post-test analyses of the wafer included analyses of plagioclase, alkali feldspar, and biotite. The feldspar data are presented graphically in Fig. 16. Complete analyses of the oxides are given in Table C6. In experiment DB16, the plagioclase varied from An_{12} to An_{36} mole%, with a pronounced maximum at An_{16-18} mole%. The composition of the K-feldspar was found to range from Or_{42} to Or_{71} mole%, with a broad maximum in the range Or_{55-68} mole%. The (FeO/FeO + Mg + MnO) × 100 ratio in the analyzed biotite was found to vary from 33 to 66, although about 80% of the values were between 58 and 66. Unfortunately, this wafer broke into two large fragments

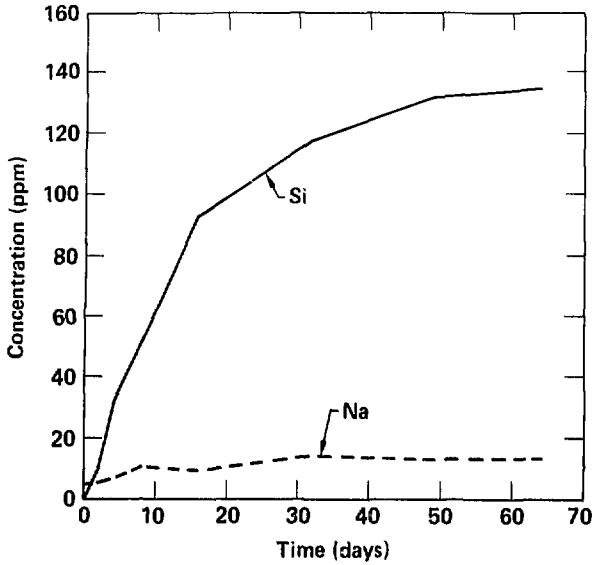

Figure 14. Fluid composition vs time for distilled water reacted with a solid polished wafer of drillcore sample Tpt G-1 1232 at 150°C in experiment DB16.

during the course of the experiment. Because these fragments were partly abraded by the rocking motion, an accurate wafer weight could not be obtained at the end of the run. An upper limit for the weight loss due to net dissolution during the run, as reflected in the dissolved silicon concentration of the fluid phase, can only be estimated roughly. If one assumes that all silicon present in solution was derived from the dissolution of cristobalite, one could produce the concentration at the end of the run by dissolving 0.058 g, or 2.4% of the wafer's initial weight, into the total amount of distilled water initially present in the gold bag.

Although the wafer broke during the experiment, the two largest fragments were recovered when the gold bag was disassembled and were cleaned and mounted in the usual way for post-test analyses of the primary phases. The surface of the wafer was also examined for secondary minerals, but no such run products were recognized. Even in the corresponding J-13 well water experiment at 150°C (DB8), only a very small amount of secondary material was produced.

The distilled water experiment run at 90°C produced very minor changes in the composition of the fluid during the course of the run. The solution was still changing in composition at the end of the run, and the steady-state estimate of composition at 90°C obviously will have to await longer-term experiments. The fluid composition is plotted versus time in Fig. 17, and the complete analyses are given in Table B9. The dissolved silicon increased linearly during the course of experiment DB17 and remained well below the solubility-limited concentration of alpha-cristobalite (49 ppm) at 90°C. The dissolved sodium content clearly rose during the experiment. The dissolved potassium also rose as a result of interaction with the water, but the analysis done on the Day 49 sample appeared to be bad. The magnesium remained nearly unchanged during the first two to four weeks, only to decrease near the end of the run. The calcium behaved similarly to the magnesium. The aluminum appeared to rise slightly during the first 48 days of the experiment but was down in the last sample. The pH rose because of interaction with the rock, but the solution had very low buffer capacity

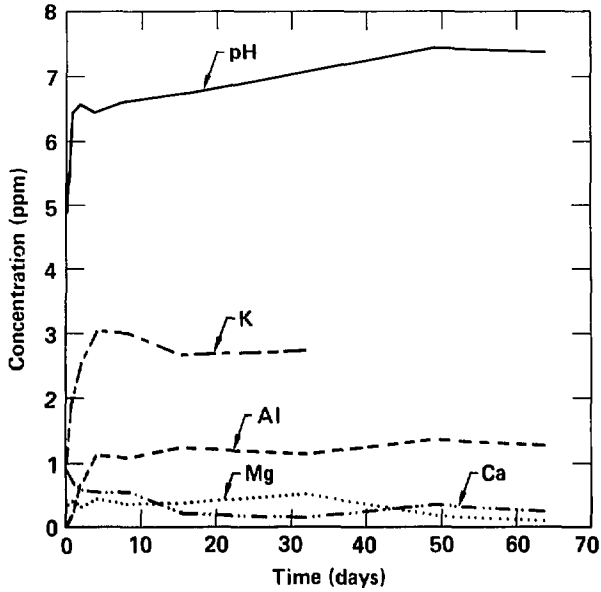

Figure 15. Fluid composition vs time for distilled water reacted with a solid polished wafer of drillcore sample Tpt G-1 1232 at 150°C in experiment DB16.

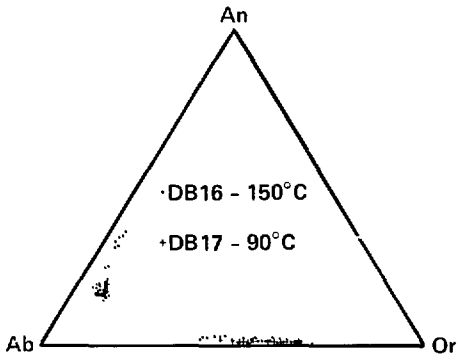

Figure 16. Composition (mole%) of coexisting feldspars following experiments DB16 and DB17 plotted in the ternary albite (Ab)-anorthite (An)-orthoclase (Or).

because the carbonate alkalinity remained very low. The anions remained uniformly low.

At the end of the run, we recovered the wafer and analyzed the primary phases. The plagioclase, K-feldspar, and biotite oxide analyses are given in Table C7. The feldspar compositions are plotted on a ternary diagram in Fig. 16. In experiment DB17, the plagioclase varied from An_{15} to An_{20} mole%, with a maximum at An_{16-17} mole%. We found that the composition of the K-feldspar varied from Or_{49} to Or_{67}. The ratio (FeO/FeO + Mg + MnO) x 100 of the analyzed biotites varied from 56 to 76, with the most common value being 68. The wafer lost 0.0162 g (0.070%) of its weight during the run.

As at 150°C, no run products were observed on the surface of the wafer at 90°C following 64 days of reaction with distilled water. Considering the limited extent of interaction, as suggested by the composition of the fluid, the absence of run products was to be expected.

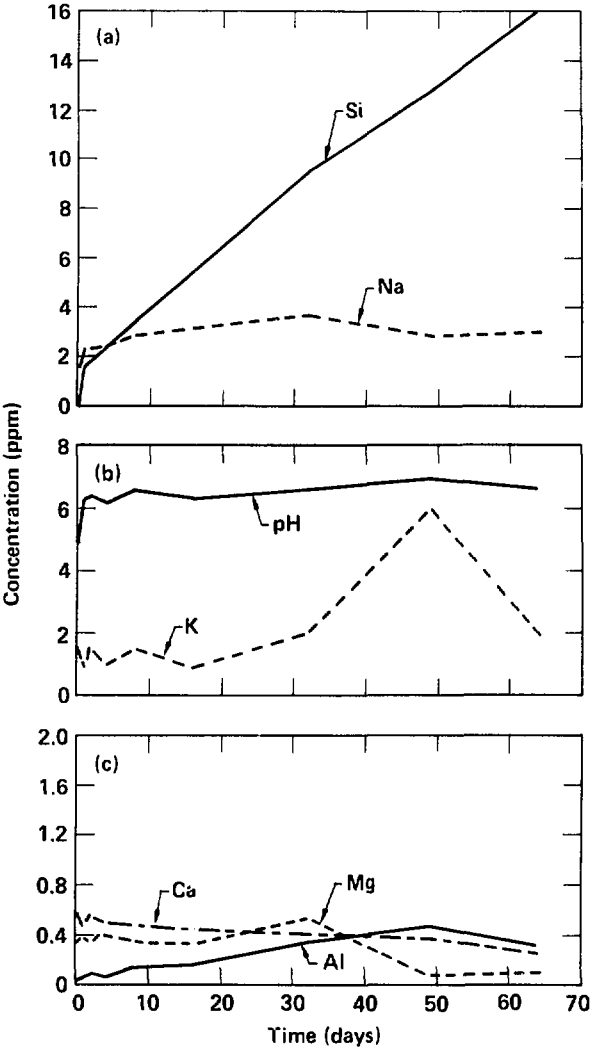

Figure 17. Fluid composition vs time for distilled water reacted with a solid polished wafer of drillcore sample Tpt G-1 at 90°C in experiment DB17. (a) Sodium and silicon; (b) potassium and pH; (c) aluminum, calcium, and magnesium.

Discussion

The expected repository conditions at Yucca Mountain include a slow infiltration rate and a low flux of water. We anticipate that interstitial water should initially be in an approximately steady-state condition with the rock and should adjust its composition during the thermal excursions caused by the disposal of radioactive waste. To determine the composition of water available to interact with the waste package and waste form, we must determine the steady-state composition of this water at various temperatures (Knauss et al., 1983). The use of crushed material to increase SA/V ratios and, hence, accelerate the rate of reaction toward a steady state in rock-water interaction experiments is a common experimental practice (Oversby, 1984a, 1984b, and 1985). The experiments performed by Knauss et al. (1985) were an attempt to use this approach (crushed tuff reacted with appropriate water at various temperatures) to determine the approximate composition of water expected to be present in the package environment. However, in these experiments with crushed tuff, the primary analytical tool for post-test analyses of the solid phases was XRD (Pawloski, 1983), which is not sensitive to the small amount of run products produced by relatively nonreactive rocks like crystalline tuff reacted at low temperatures. Thus, to infer the run products produced, we must use a geochemical reaction-path modeling code (EQ3/6); this has been done for experiments with crushed tuff at 150°C (Delany, 1985). To confirm the mineral assemblage predicted by the modeled rock-water interaction, we must know the identity and chemical character of the run products actually produced at each temperature.

By using solid, polished wafers of tuff in these experiments, we have provided a convenient surface upon which to grow the run products. Post-test analyses of the surface of the reacted waters offers a better opportunity to identify, or at least narrow the range of, potential minerals comprising the assemblage of secondary minerals formed as a result of the hydrothermal interactions. The results of these analyses have been presented in some detail in the results section and in Appendices D and E.

The 150°C polished wafer experiment (DB8) was modeled by Delaney (1985), using EQ6. After minor adjustments were made to the input parameters (e.g., SA/V), dissolution rates, etc., permissible within the range of uncertainty of the starting parameters, a reasonably good fit was obtained between the actual fluid composition observed in the experiment and the modeled fluid composition produced by EQ6 (Knauss et al., 1984). The modeled product phases were found to be calcium-smectite, cristobalite, and a small amount of calcium-zeolite. Early in the modeled experiment, calcite was supersaturated briefly but became understaturated as the run progressed. In the actual experiment, the secondary phases were dominated by claylike phases and rare gibbsite (or boehmite) and cristobalite. Considering the limited choice of phases (and ranges in their composition) available to precipitate in the EQ3/6 data base, it is not unreasonable, theoretically, that a small amount of zeolite could form. Conversely, given more time, the actual experiment may have produced zeolites if they were kinetically inhibited from precipitating. The version of the code used makes no allowances for precipitation kinetics; once a phase is supersaturated, it is assumed to precipitate instantaneously. In fact, a subsequent report (Knauss et al., 1987) shows that a calcium-bearing, silicon-rich zeolite did precipitate in minor amounts during a long-term (303-day) experiment run under identical conditions. Nevertheless, the agreement between the modeled results at 150°C and the actual experiment is remarkably good.

The 250°C polished wafer experiment (DB9) was also modeled by Delaney (1985), using EQ6. The phases present as reactants were the same at both 150 and 250°C. Again, minor changes in the SA/V ratio and dissolution rates produced a modeled fluid phase whose evolution with time, in most respects, resembled the fluid actually observed in the experiment. The notable exception was aluminum; apparently, there was no precipitated phase in the EQ3/6 simulation to account for the observed decrease in aluminum concentration following the initial pulse. As at 150°C, the initial pulse in potassium was not produced in the simulation. In general, the simulation at 250°C did not agree as well with the observed fluid concentrations or observed run products as that at 150°C. The reaction products generated in the EQ3/6 simulation were calcium-smectite and lesser clinoptilolite, which are opposites of the relative proportions one would expect on the basis of the Oswald-step rule (Dibble and Tiller, 1981) and of the proportions actually observed in the hydrothermal experiment. In experiment DB9, the run products were dominated by the zeolites dachiardite and mordenite, with very minor amounts

of a claylike phase and cristobalite. Obviously, a more complete data base, particularly for the zeolites, is required before EQ3/6 can adequately model hydrothermal systems at temperatures up to 250°C.

A comparison of results obtained in analogous experiments using crushed drillcore tuff (Knauss et al., 1985) with those obtained here using solid wafers of tuff at all three temperatures (90, 150, and 250°C) shows generally good agreement. The main difference is that the rate at which most constituents were released was accelerated in the crushed tuff experiments. In some cases, the final solution concentrations were also slightly higher for some elements in the crushed tuff experiments.

At 150°C, for example, the silicon concentration rose more rapidly in the crushed tuff experiment than it did in the solid wafer experiment and reached a concentration that was about 14% higher than the concentration expected for solubility control by cristobalite (Fournier and Rowe, 1962; Walther and Helgeson, 1977). By the end of the run in the wafer experiments, the silicon concentration had just reached cristobalite solubility. It should be noted, however, that the silicon concentration had not leveled off to a well-established steady-state value even by the end of the run in the wafer experiment and still appeared to be rising slightly. This continued increase in silicon with time was confirmed in later long-term experiments with wafers (Knauss et al., 1987). The potassium and aluminum concentrations displayed the same trends in both the crushed tuff and wafer experiments, although the initial pulse in both cases was more pronounced in the crushed tuff experiments. The sodium also rose to a higher value by the end of the crushed tuff experiment.

At 250°C, the silicon again increased more rapidly in the crushed tuff experiment than it had in the wafer experiment. However, the final concentration of silicon was essentially equal to that determined by solubility control by cristobalite. For most of the other dissolved constituents, this agreement between the crushed tuff and wafer experiments at 250°C was much better. The initial pulses in potassium and aluminum and the initial drop in calcium were much more similar in both experiments at 250°C. Apparently the rates of dissolution at 250°C were increased to such an extent that they overshadowed the effect of a diminished effective surface area in the wafer experiments compared with the experiments using crushed tuff.

At 90°C, the extent of reaction was so minor that it is difficult to make this comparison between the wafer and crushed tuff experiments. Nevertheless, the trends in the dissolved elements were similar, although developed to a greater degree in the crushed tuff experiment. The most noticeable difference appeared to be in the potassium and aluminum concentrations produced in solution. These elements increased considerably in the crushed tuff experiment and much more slowly and to a lesser degree in the wafer experiment.

In the report on hydrothermal interaction of J-13 water with crushed tuff (Knauss et al., 1985), we attempted to estimate a steady-state water composition based on the short-term experiments. The results obtained here generally conform to those estimates although, for some elements, especially those at 90 and 150°C, it is clear that the effect of the decreased reactivity of the wafers was a decrease in the extent of reaction over the same time period. Better estimates of this steady-state water composition can be made by making long-term experiments at the same temperatures. In recently completed experiments, wafers of tuff were reacted with J-13 water for 303 days at 90 and 150°C (Knauss et al., 1987).

The use of J-13 water as a reference water for predicting the altered water composition within the nearfield is not an unreasonable approximation. A comparison of results obtained with J-13 water and distilled water will bear this out. In fact, in some ways, the use of J-13 water may be more appropriate than using distilled water because some dissolved constituents expected to be present in the pore water within the unsaturated zone at Yucca Mountain are removed from solution by hydrothermal interaction with the rock. These species are not present in distilled water and, therefore, are not available to form run products.

A greatly simplified explanation based solely on aqueous phase results obtained in the analogous crushed tuff experiments (Knauss et al., 1985) was provided to explain the chemical evolution of fluid in contact with tuff and to predict the reaction products that could be expected to form as a result of the tuff-water interaction. Using the results obtained with wafers of tuff, we have confirmed the chemical evolution of the fluid phase and provided details on the reaction products that actually resulted from the interaction. In general, these results confirm the nature of the reaction products proposed above.

As we pointed out earlier for crushed tuff, the trends observed in the chemical evolution of the fluids at 90, 150, and 250°C were consistent; the

main effe . of temperature appeared to be an increase in the rate at which these trends develop with time. This fact might be used to argue that the mechanisms involved in both the dissolution of primary phases and the precipitation of reaction products are the same at the three temperatures. If the argument is valid, increasing temperature alone could provide a method by which these tuff-water interactions could be accelerated to say something about long-term interactions at lower temperatures.

Although the rates of reaction will obviously be more rapid in particular rock-water systems at higher temperatures, it is not clear that the reaction products resulting from the high-temperature interaction will resemble the reaction products that are expected to exist at lower temperatures. Jenkins et al. (1984) previously noted the potential dangers in making this assumption about the reaction products and the consequences that result from making predictions about waste form performance on the basis of such accelerated tests. To determine if this method of accelerating tests is valid for waste package environment experiments pertinent to a potential repository at Yucca Mountain, we must identify the run products and characterize their compositions. The tuff-water interaction experiments run using solid core wafers in the Dickson-type gold-bag rocking autoclaves, the subject of this report, are a first attempt to provide precisely this information.

What we have observed with respect to the nature and composition of reaction products as a function of temperature in the short-term experiments would, in fact, lead us to conclude that the same mechanisms might not be operative at 90, 150, and 250°C. For example, at 150°C we observed that the run products were dominated by claylike phases, while at 250°C they were dominated by zeolites. However, if the growth of zeolites was kinetically inhibited at 150°C, the zeolites might actually dominate at 150°C if the experiment were allowed to continue for a sufficiently longer period of time. This is the case; it will be described in a subsequent report on long-term hydrothermal interaction experiments.

The preliminary EQ6 results obtained by Delany (1985) in modeling the short-term experiments suggest that further experimental work is required before the processes that control the composition of the fluid phase can be understood. In all crushed tuff experiments, the initial release rate for silicon exceeds that predicted by the model. This same effect is not seen in the wafer experiments, perhaps because of the presence of ultrafine material adhering to the crushed tuff. This ultrafine material has been shown to produce an initial parabolic release rate (Holdren and Berner, 1979; Petrovich, 1981) that cannot be normalized by SA/V manipulations based on BET gas-adsorption surface-area measurements. Work done by Oversby (1985) in which crushed tuff was pretreated by reacting with J-13 water at run temperature and then restarted with fresh solution has shown, in most cases, that there is an initial rapid silicon release, probably the result of dissolution of an ultrafine fraction. Additional experiments should be made using pretreated crushed tuff whose ultrafines have been removed by vigorous mechanical cleaning with isopropanol, at room temperature, using an ultrasonic bath (Knauss and Wolery, 1986). The dissolution rate should be monitored closely during the early stages of reaction. Such experiments should quantify the magnitude of this ultrafine effect.

In the experiments with crushed tuff or wafers of tuff, there was an initial pulse in both aluminum and potassium. The aluminum pulse was simulated by allowing very rapid dissolution of a montmorillonite phase as an aluminum source. However, the potassium pulse was more enigmatic and could be controlled thermodynamically rather than kinetically (Delany, 1985). Hydrothermal experiments in which the rock-water ratio is varied may help to decipher the behavior of potassium. In the wafer experiments, the rock-water ratio (mass) was approximately 0.035. Experiments can easily be run with ratios up to about 1.0, or some 30 times higher than the ratio in the wafer experiments presented in this report.

At present, we do not know the rate at which run products formed during the experiments. While it is obvious that the two zeolites (dachiardite and mordenite) in the 250°C experiment are contemporaneous, we do not know if they formed early in the run and then remained stable throughout the remainder of the run or whether they grew continuously during the course of the experiment. Because the wafer was extracted at the end of the run, following the quench of the vessel, we have no way of knowing. To monitor the development of run products with time, a series of analogous experiments should be performed in cold-seal pressure vessels. These experiments could be run under conditions identical to those reported here, only with no fluid sampling during the course of the experiment. Rather, a series of identical pressure vessels could be assembled and opened progressively with time. In

this sense, the proposed experiments are complementary to those reported herein. While experiments in the Dickson-type autoclaves can provide the chemistry of evolving fluid without quench effects, they can only provide information on the secondary mineral assemblage present at the end of the run. In like manner, cold-seal pressure vessel experiments cannot provide information on the evolving fluid chemistry without the risk of quench effects, but can provide information on the evolving secondary mineral assemblage.

As described above, the run products in some of the experiments may not be categorized unambiguously as either true secondary minerals from the hydrothermal interaction at elevated temperatures or products that grew during the quench at the end of the experiment. This is particularly true of the minor amounts of claylike phases found covering the zeolites and other more obvious run products formed in the 250°C experiments. To make this distinction, we believe that a limited number of experiments duplicating those reported herein should be carried out but should be followed by a rapid quench to room temperature. At higher temperatures (250°C and above), rapid quenching of thicked-walled vessels of this size (containing 1000 ml of fluid) can be rather stressful to the pressure vessel; therefore, these rapid-quench experiments should be done in cold-seal vessels.

Acknowledgments

We wish to thank Bob Rosenbauer of the United States Geological Survey, Menlo Park, and Bill Seyfreid of the University of Minnesota for their valuable advice on how to avoid pitfalls in setting up the Dickson-type autoclaves. Thanks also go to Bob Rosenbauer for information regarding the infrared CO_2 analyzer for carbonate analysis, to Jay Alexander for plumbing in the pressure lines to the racks, and to Carl Boro for remachining pressure vessel parts. Art Langhorst and Winnie Burks made the ICP-ES measurements on the direct reading unit, Terry Duewer and Sandy Fadeff made the measurements on the sequential unit, and Jackie Lam made the IC measurements. Bob Lim and Jeff Haas made AA measurements, and Chuck Slettevold and Suzie Saunders did the BET analyses.

References

Bish, D. L., F. A. Caporuscio, J. F. Copp, B. M. Crowe, J. D. Purson, J. R. Smyth, and R. S. Warren (1981), *Preliminary Stratigraphic and Petrologic Characterization of Core Samples from USW G-1, Yucca Mountain, Nevada*, Los Alamos National Laboratory, Los Alamos, NM, LA-8840-MS.

Byers, F. M. (1984), Los Alamos National Laboratory, Los Alamos, NM, personal communication.

Delany, J. M. (1985), *Reaction of Topopah Spring Tuff with J-13 Water: A Geochemical Modeling Approach Using the EQ3/6 Reaction Path Code*, Lawrence Livermore National Laboratory, Livermore, CA, UCRL-53631.

Dibble, W. E., and W. A. Tiller (1981), "Kinetic Model of Zeolite Paragenesis in Tuffaceous Sediments," *Clays and Clay Miner.* **29**, 323–330.

Engels, J.C. (1972), "Determination of Purity of Mineral Separates Used in K-Ar Dating—An Interpretive Review," *Can. Miner.* **11**, 743–759.

Fournier, R. D., and J. J. Rowe (1962), "The Solubility of Cristobalite Along the Three-Phase Curve, Gas Plus Liquid Plus Cristobalite," *Am. Miner.* **47**, 897–902.

Holdren, G. R., and R. A. Berner (1979), "Mechanism of Feldspar Weathering—I. Experimental Studies," *Geochim. Cosmochim. Acta* **43**, 1161–1171.

Jenkins, D. M., J. R. Holloway, and J. F. Kacoyannakis (1984), "Temporal Variations of Aqueous Constituents in a Water-Basalt-Supercalcine System: Implications for the Experimental Assessment of Nuclear Waste Forms," *Geochim. Cosmochim. Acta* **48**, 1443–1454.

Knauss, K. G. (1984), *Petrologic and Geochemical Characterization of the Topopah Spring Member of the Paintbrush Tuff: Outcrop Samples Used in Waste Package Experiments*, Lawrence Livermore National Laboratory, Livermore, CA. UCRL-53558.

Knauss, K. G. (1985), Lawrence Livermore National Laboratory, Livermore, CA, unpublished data.

Knauss, K. G., and W. J. Beiriger (1984), *Report on Static Hydrothermal Alteration Studies of Topopah Spring Tuff Wafers in J-13 Water at 150°C*, Lawrence Livermore National Laboratory, Livermore, CA, UCRL-53576.

Knauss, K. G., and W. J. Beiriger (1984b), "Dachiardite Formation by Hydrothermal Alteration of a Devitrified High-Silica Rhyolite," *Geol. Soc. Am. Prog. Abstr.* **16** (6), 561.

Knauss, K. G., W. J. Beiriger, and D. W. Peifer (1985), *Hydrothermal Interaction of Crushed Topopah Spring Tuff and J-13 Water at 90°C, 150°C, and 250°C Using the Dickson-Type Gold-Bag Rocking Autoclave*, Lawrence Livermore National Laboratory, Livermore, CA, UCRL-53630.

Knauss, K. G., W. J. Beiriger, and D. W. Peifer (1987), *Hydrothermal Interaction of Solid Wafers of Topopah Spring Tuff with J-13 Water at 90°C and 150°C Using the Dickson-Type Gold-Bag Rocking Autoclaves: 2. Long-Term Experiments*, Lawrence Livermore National Laboratory, Livermore, CA, UCRL-53722.

Knauss, K. G., J. D. Delany, W. J. Beiriger, and D. W. Peifer (1984), "Hydrothermal Interaction of Topopah Spring Tuff with J-13 Water as a Function of Temperature," *Mat. Res. Soc. Symp. Proc.* **44**, 539–546. Also see Lawrence Livermore National Laboratory, Livermore, CA, UCRL-90853, 1984.

Knauss, K. G., V. M. Oversby, and T. J. Wolery (1983), "Post Emplacement Environment of Waste Packages," *Mat. Res. Soc. Symp. Proc.* **26**, 301–308.

Knauss, K. G., and T. J. Wolery (1986), "Dependence of Albite Dissolution Kinetics on pH and Time at 25°C and 70°C," *Geochim. Cosmochim. Acta* **50**, 2481–2497.

Oversby, V. M. (1984a), *Reaction of Topopah Spring Tuff with J-13 Well Water at 90°C and 150°C*, Lawrence Livermore National Laboratory, Livermore, CA, UCRL-53552.

Oversby, V. M. (1984b), *Reaction of Topopah Spring Tuff with J-13 Well Water at 120°C*, Lawrence Livermore National Laboratory, Livermore, CA, UCRL-53574.

Oversby, V. M. (1985), *Reaction of Topopah Spring Tuff from Drillcore USW G-1, USW GU-3, USW G-4, and UE-25h#1 with J-13 Water at 150°C*, Lawrence Livermore National Laboratory, Livermore, CA, UCRL-53629.

Oversby, V. M., and K. G. Knauss (1983), *Reaction of Bullfrog Tuff with J-13 Water at 90°C and 150°C*, Lawrence Livermore National Laboratory, Livermore, CA, UCRL-53442.

Passaglia, E. (1970), "The Crystal Chemistry of Chabazites," *Am. Miner.* **55**, 1278–1301.

Pawloski, G. A. (1983), *Quantitative Determination of Minerals in Nevada Test Site Samples by X-Ray Diffraction*, Lawrence Livermore National Laboratory, Livermore, CA, UCRL-89414.

Petrovich, R. (1981), "Kinetics of Mechanically Comminuted Rock-Forming Oxides and Silicates—I. Deformation and Dissolution of Quartz Under Laboratory Conditions," *Geochim. Cosmochim. Acta*, **45**, 1665–1674.

Schuraytz, B. (1985), *Geochemical Gradients in the Topopah Spring Member of the Paintbrush Tuff: Evidence for Eruption Across a Magmatic Interface*, Lawrence Livermore National Laboratory, Livermore, CA, UCRL-53698.

Seyfreid, W. E., R. C. Gordon, and F. W. Dickson (1979), "A New Reaction Cell for Hydrothermal Solution Equipment," *Am. Miner.* **64**, 646–649.

Stein, W., J. N. Hockman, and W. C. O'Neal (1984), *Thermal Analysis of NNWSI Conceptual Waste Package Designs*, Lawrence Livermore National Laboratory, Livermore, CA, UCID-20091.

Travis, B. J., S. W., Hodson, H. E. Nuttal, T. L. Cook, and R. S. Rundberg (1984), *Preliminary Estimates of Water Flow and Radionuclide Transport in Yucca Mountain*, Los Alamos National Laboratory, Los Alamos, NM, LA-UR 84-40 (Rev.).

Walther, J. V., and H. C. Helgeson (1977), "Calculation of the Thermodynamic Properties of Aqueous Silica and the Solubility of Quartz and its Polymorphs at High Temperatures and Pressures," *Am. J. Sci.* **277**, 1315–1351.

Walther, J. V., and P. M. Orville (1983), "The Extraction-Quench Technique for Determination of the Thermodynamic Properties of Solute Complexes: Application to Quartz Solubility in Fluid Mixtures," *Am. Miner.* **68**, 731–741.

Warren, R. S., F. M. Byers, and F. A. Caporuscio (1984), *Petrography and Mineral Chemistry of Units of the Topopah Spring, Calico Hills, and Crater Flat Tuffs, and Older Volcanic Units, with Emphasis on Samples from Drill Hole USW G-1, Yucca Mountain, Nevada Test Site*, Los Alamos National Laboratory, Los Alamos, NM, LA-10003-Ms.

MLD/mp

Appendix A. Electron Microprobe Analyses of Unreacted Tuff

Appendix B. Fluid Phase Analyses

Appendix C. Electron Microprobe Analyses of Reacted Tuff

Appendix D. Crystallography and Chemistry of Dachiardite Produced at 250°C (Experiments DB7 and DB9)

Introduction

Scanning electron microscope observations of the surface of the reacted wafers from experiments DB7 and DB8 indicated that the secondary minerals present were large enough to be plucked from the surface of the wafer for more detailed characterization. This was performed by using a binocular microscope and a dissecting needle dabbed with alcohol. One crystal mass was mounted on the end of a glass fiber and prepared for XRD analysis using a Gandolfi camera. Many other crystal masses were plucked from the surface of the wafer and used to prepare an epoxy grain mount. The crystals were confined within a stainless steel nut that was floated in the partially set epoxy. By carefully polishing the grain mount, we were able to remove the overlying epoxy and expose the crystals at the surface. This polished grain mount was suitable for quantitative analyses using WDS techniques on the EMP.

The dominant secondary mineral formed as a result of the hydrothermal interaction of this densely welded, devitrified ashflow tuff (compositionally a high-silica rhyolite) with a dilute ($Na + HCO_3$) ground water at 250°C was the rare zeolite dachiardite. Dachiardite is a mordenite-group, high-silica zeolite with a cation content similar to that of mordenite, with which it is commonly associated (Wise and Tschernich, 1978). The type locality for dachiardite is a hydrothermally altered zone in a pegmatite near San Piero di Campo, Elba, Italy (Bonardi, 1979). Its generalized compositon is given as

$$(Ca_{1.2}, Na, K)_5[Al_5Si_{19}O_{48}] \cdot 12\ H_2O$$

The type locality mineral was rich in calcium (Ca/Na + K = 1.23). Since its original reporting by D'Archiardi in 1906, this mineral has only been observed in a few other localities, but almost always as a sodium-rich endmember. Sodium-rich daciardite has been reported in Alpe di Siusi, Italy (Alberti, 1975); in Tsugawa, Japan (Yoshimura and Nakabayushi, 1977); in Washington and Oregon (Wise and Tschernich, 1978); in Chichijima, Japan (Nishido et al., 1979); and in the Francon Quarry, Montreal, Quebec (Bonardi et al., 1981). The only other locality with reportedly calcium-rich dachiardite is at Yellowstone National Park (Barger and Beeson, 1981; Barger et al., 1981; Barger, 1984), where dachiardite occurs in hydrothermally altered, rhyolitic, pumiceous tuff and lava.

The dachiardite structure has been studied by Gellens et al. (1982), but little is known about its cation exchange properties, thermal stability (only the sodium-rich variety has been studied in any detail), etc. There are no known reports of its synthesis from oxides, nor has it been reported as a run product of hydrothermal rock-water interaction in any published laboratory experiments.

X-Ray Diffraction Identification and Calculation of Cell Constants Using the Gandolfi Camera

We plucked a rosette of crystals from the surface of the reacted wafer and mounted it on a glass rod for exposure to CuK_α radiation within a Gandolfi camera. This camera rotates samples approximately 45° during exposure, as well as rotating the film on the focal plane. The d-spacings of lines recorded on the exposed film from the Gandolfi camera are listed in Table D1. As can be seen, the match to the type locality dachiardite was excellent. A linear regression of the XRD data allowed the calculation of cell constants (Appleman, 1963). The refined cell constants for the dachiardite produced in experiments DB7 and DB9 and those of the type locality were as follows.

	Elba		Dachiardite run product
a_o	18.685 Å	a_o	18.645 Å
b_o	7.495 Å	b_o	7.483 Å
c_o	10.260 Å	c_o	10.247 Å
V_o	1367 Å^3	V_o	1358 Å^3
β	107°54′	β	108°09′

Table D1. XRD data for the type locality dachiardite and the unknown run product.

Elba dachiardite (JCPDS card 18-467) d (Å)[a]	I[b]	Miller indices	Unknown run product d (Å)
9.79	10	001	9.75
8.90	50	200	8.88
6.91	50	110	6.90
6.00	35	111	6.00
5.35	20	111	5.30
4.97	50	202	4.95
4.88	50	002	4.88
4.61	10	401	4.62
4.45	10	400	4.42
4.23	10	112	4.22
3.932	50	402	3.95
3.801	50	202	3.80
3.634	20	401	3.63
3.452	100	220	3.45
3.328	35	511	3.33
3.204	100	510	3.20
2.964	50	602	2.96
2.862	50	402,420	2.86
2.712	50	422	2.72
2.666	50	222	2.66
2.550	50	204	2.56
2.387	20	512, 621	2.39
2.306	20	403, 331	2.30
2.273	10	713, 514	2.29
1.873	75		1.87
1.776	35		1.77

[a] d(Å) = d-spacing (ergstroms).
[b] I = relative intensity.

The other run products produced in experiments DB7 and DB9 were less abundant and too small to allow similar XRD identification.

EMP/XRD Quantitative Analyses

We hand-picked the largest prismatic crystals and rosettes of dachiardite from the surface of the reacted wafer and prepared a polished grain mount for quantitative WDS analyses. To minimize volatile

loss, we made the analyses at 15 kV and 5-nA sample current, using a 25-μ^2 rastered beam and a total beam time of less than 75 s for a nine-element analysis. These analyses were made on a fully automated JEOL 733 electron microprobe with a beam stabilizer. This microprobe uses beam blanking during spectrometer rotation and computer-determined order-of-element analysis to minimize the beam time on the sample.

In spite of the analytical precautions, it was difficult to analyze zeolite minerals quantitatively with an electron microprobe. A total of 71 WDS analyses were attempted on this grain mount, but only 45 were accepted as good analyses. The criterion for acceptance consists of an error function (E) that is a balance of total alkalis vs aluminum (Passaglia, 1970). For an analysis to be acceptable, E must be less than ±7%, where

$$E = \frac{Al_{observed} - Al_{theoretical}}{Al_{theoretical}} \times 100$$

and $Al_{theoretical} = Na + K + 2(Ca + Mg)$. Another integral check is to ensure that the sum (Al + Si) equals 24 in the unit cell of 48 oxygens. Both of these checks were applied to the analyses, and the data given in the EMP analyses tables were acceptable by both criteria.

Because the dachiardite analyses were made on crystals plucked from two separate wafers of Tpt tuff (drillcore and outcrop) exposed to well J-13 ground water at 250°C for 64 days and the experiments were run at slightly different pressures (DB7 = 100 bars and DB9 = 50 bars), we decided to treat the data initially as though they were from two separate populations. The results of the quantitative analyses, presented both as oxides and as cations calculated on the basis of 48 oxygens, are given in Tables D2 and D3 for experiments DB9 and DB7, respectively. For each experiment, we made separate histograms of the number of cations per 48 oxygens for the elements Si, Al, Ca, K, and Na and compared the mean and standard deviation in the mean. The results of this comparison were as follows.

	DB9	DB7	Combined
Si	19.15 ± 0.18	19.15 ± 0.16	19.15 ± 0.18
Al	4.88 ± 0.16	4.87 ± 0.17	4.87 ± 0.17
Ca	2.12 ± 0.10	2.07 ± 0.12	2.10 ± 0.11
K	0.30 ± 0.05	0.38 ± 0.09	0.34 ± 0.07
Na	0.16 ± 0.07	0.17 ± 0.06	0.16 ± 0.08

It is readily apparent that the compositions represented are identical. For the remainder of this discussion, we will treat the 45 analyses as one population, regardless of whether they come from experiment DB9 or DB7. The alkali cation content based on 48 oxygens is shown in a ternary diagram (Na–K–Ca) in Fig. D1.

We calculated the water of hydration by difference, using the average compositon and average analytical total of oxides (85.94 ± 2.53%). On the basis of 45 reliable quantitative WDS analyses, the formula for the dachiardite produced in these experiments was

$$Ca_{2.10}K_{0.34}Na_{0.16}(Al_{4.87}Si_{19.15}O_{48}) \cdot 13.9\ H_2O$$

Using this hydrated formula weight and the cell volume from the XRD analysis, we calculated a density of 2.18 g/cm^3. The measured density for the Elba dachiardite was 2.17 g/cm^3. The waters of hydration reported in the literature range from 12.4 to 14.2 for sodium-rich dachiardite, while the type locality (calcium-rich) dachiardite contained 12.7 waters.

Table D2. Quantitative WDS analyses from DB9.

Unknown: Wt % Pt#	Oxides Si	Al	Na	K	Ca	Mg	Ti	Fe	Mn	Sum
1	62.13	13.96	0.56	0.77	6.67	0.04	0.00	0.04	0.00	84.17
2	62.00	14.38	0.44	0.06	6.83	0.00	0.02	0.02	0.00	84.35
3	63.49	13.54	0.38	0.92	6.13	0.00	0.07	0.04	0.02	84.59
4	60.44	13.85	0.35	0.83	6.43	0.00	0.00	0.06	0.00	81.96
5	63.73	13.40	0.21	0.77	6.37	0.00	0.00	0.03	0.00	84.51
6	64.90	13.74	0.38	0.55	6.72	0.01	0.00	0.07	0.00	86.37
7	64.33	13.42	0.24	0.84	6.51	0.00	0.00	0.00	0.00	85.34
8	60.63	13.37	0.36	0.92	6.00	0.00	0.11	0.00	0.00	81.39
10	59.23	13.00	0.30	0.80	6.08	0.00	0.00	0.00	0.00	79.41
12	61.75	14.53	0.27	0.53	6.94	0.00	0.00	0.06	0.00	84.08
13	63.31	13.98	0.27	0.75	6.48	0.00	0.05	0.04	0.02	84.90
14	62.17	14.13	0.20	0.55	7.36	0.00	0.00	0.03	0.05	84.49
15	62.58	13.46	0.24	0.93	6.69	0.00	0.00	0.02	0.00	83.92
16	60.50	12.45	0.10	0.86	5.96	0.01	0.01	0.07	0.00	79.96
24	64.78	14.18	0.37	0.97	6.49	0.01	0.12	0.10	0.00	87.02
29	62.63	12.86	0.17	0.78	6.12	0.00	0.00	0.11	0.04	82.71
31	66.97	13.67	0.17	0.91	6.48	0.03	0.00	0.12	0.58	88.93
32	65.07	14.05	0.22	0.64	6.99	0.00	0.00	0.11	0.00	87.08
33	64.22	14.19	0.20	0.71	6.77	0.04	0.00	0.05	0.04	86.22
35	68.24	13.32	0.08	0.75	6.51	0.00	0.00	0.05	0.02	88.97
37	63.90	12.96	0.00	0.80	6.04	0.00	0.00	0.00	0.06	83.76

Structural formula based on 48.00 oxygens

Pt#	Si	Al	Na	K	Ca	Mg	Ti	Fe	Mn	Sum
1	18.97	5.02	0.33	0.30	2.18	0.02	0.00	0.01	0.00	26.83
2	18.88	5.16	0.26	0.26	2.23	0.00	0.00	0.01	0.00	26.79
3	19.22	4.83	0.22	0.36	1.99	0.00	0.02	0.01	0.01	26.64
4	18.94	5.12	0.21	0.33	2.16	0.00	0.00	0.02	0.00	26.77
5	19.28	4.78	0.12	0.30	2.06	0.00	0.00	0.01	0.00	26.55
6	19.22	4.80	0.22	0.21	2.13	0.00	0.00	0.02	0.00	26.60
7	19.28	4.74	0.14	0.32	2.09	0.00	0.00	0.00	0.00	26.58
8	19.09	4.96	0.22	0.37	2.02	0.00	0.03	0.00	0.00	26.69
10	19.11	4.94	0.19	0.33	2.10	0.00	0.00	0.00	0.00	26.67
12	18.85	5.23	0.16	0.21	2.27	0.00	0.00	0.02	0.00	26.72
13	19.10	4.97	0.16	0.29	2.09	0.00	0.01	0.01	0.01	26.63
14	18.91	5.07	0.12	0.21	2.40	0.00	0.00	0.01	0.01	26.72
15	19.14	4.85	0.14	0.36	2.19	0.00	0.00	0.01	0.00	26.69
16	19.34	4.69	0.06	0.35	2.04	0.00	0.00	0.02	0.00	26.51
24	19.10	4.93	0.21	0.36	2.05	0.00	0.03	0.02	0.00	26.70
29	19.35	4.68	0.10	0.31	2.03	0.00	0.00	0.03	0.01	26.51
31	19.31	4.65	0.10	0.33	2.00	0.01	0.00	0.03	0.14	26.58
32	19.14	4.87	0.13	0.24	2.20	0.00	0.00	0.03	0.00	26.61
33	19.08	4.97	0.12	0.27	2.16	0.02	0.00	0.01	0.01	26.63
35	19.54	4.50	0.04	0.27	2.00	0.00	0.00	0.01	0.00	26.37
37	19.44	4.65	0.00	0.31	1.97	0.00	0.00	0.00	0.02	26.39

Table D3. Quantitative WBS analyses from DB7.

Unknown:

Wt % Pt#	Oxides Si	Al	Na	K	Ca	Mg	Ti	Fe	Mn	Sum
1	65.01	13.59	0.04	1.12	6.31	0.00	0.07	0.09	0.00	86.23
2	64.47	13.56	0.15	0.86	6.75	0.01	0.00	0.06	0.00	85.86
5	63.03	14.43	0.49	0.69	7.01	0.00	0.03	0.12	0.01	85.81
6	64.53	14.29	0.75	0.78	6.73	0.03	0.00	0.18	0.00	87.29
7	63.88	13.71	0.21	1.24	6.45	0.00	0.00	0.06	0.00	85.55
11	66.60	13.58	0.16	1.06	6.41	0.00	0.00	0.02	0.00	87.83
12	65.83	13.40	0.20	0.96	6.29	0.00	0.00	0.07	0.00	86.75
13	64.78	13.63	0.27	1.22	6.23	0.00	0.01	0.02	0.00	86.16
14	65.50	13.69	0.39	1.29	6.21	0.06	0.00	0.05	0.00	87.19
15	65.43	13.97	0.21	0.97	6.53	0.00	0.00	0.02	0.03	87.16
16	65.82	13.69	0.25	1.14	6.51	0.01	0.00	0.00	0.02	87.44
17	69.42	14.57	0.19	0.55	7.22	0.00	0.00	0.00	0.09	92.04
18	65.72	15.00	0.19	0.64	7.04	0.00	0.00	0.00	0.82	89.41
20	67.75	14.28	0.30	0.93	6.47	0.02	0.00	0.00	0.07	89.82
22	64.34	14.36	0.32	1.09	6.39	0.02	0.01	0.05	0.06	86.64
23	63.05	14.43	0.29	0.68	7.31	0.02	0.00	0.05	0.00	85.83
24	64.43	13.96	0.53	1.60	6.02	0.17	0.00	0.08	0.04	86.83
26	63.71	14.30	0.19	0.97	6.87	0.06	0.01	0.05	0.00	86.16
28	68.81	14.48	0.34	1.08	6.56	0.02	0.11	0.00	0.05	91.45
29	62.96	14.24	0.31	1.16	7.07	0.04	0.05	0.06	0.00	85.89
30	64.89	13.46	0.31	1.21	6.49	0.00	0.11	0.00	0.04	86.51
31	64.08	12.92	0.27	1.02	5.91	0.04	0.00	0.05	0.04	84.33
32	63.09	14.46	0.42	0.89	6.88	0.00	0.00	0.00	0.00	85.74
33	64.41	14.84	0.35	0.79	7.09	0.02	0.09	0.08	0.06	87.73

Structural formula based on 48.00 oxygens

Pt#	Si	Al	Na	K	Ca	Mg	Ti	Fe	Mn	Sum
1	19.29	4.75	0.02	0.42	2.01	0.00	0.02	0.02	0.00	26.54
2	19.23	4.77	0.09	0.33	2.16	0.00	0.00	0.01	0.00	26.59
5	18.89	5.10	0.28	0.26	2.25	0.00	0.01	0.03	0.00	26.83
6	19.01	4.96	0.43	0.29	2.12	0.01	0.00	0.04	0.00	26.87
7	19.17	4.85	0.12	0.47	2.07	0.00	0.00	0.02	0.00	26.70
11	19.38	4.66	0.09	0.39	2.00	0.00	0.00	0.00	0.00	26.53
12	19.39	4.65	0.11	0.36	1.99	0.00	0.00	0.02	0.00	26.52
13	19.27	4.78	0.16	0.46	1.99	0.00	0.00	0.00	0.00	26.65
14	19.27	4.75	0.22	0.48	1.96	0.03	0.00	0.01	0.00	26.71
15	19.22	4.84	0.12	0.36	2.06	0.00	0.00	0.00	0.01	26.61
16	19.29	4.73	0.14	0.43	2.04	0.00	0.00	0.00	0.00	26.63
17	19.27	4.77	0.10	0.19	2.15	0.00	0.00	0.00	0.02	26.50
18	18.91	5.09	0.11	0.23	2.17	0.00	0.00	0.00	0.20	26.71
20	19.28	4.79	0.17	0.34	1.97	0.01	0.00	0.00	0.02	26.57
22	19.06	5.01	0.18	0.41	2.03	0.01	0.00	0.01	0.02	26.73
23	18.89	5.09	0.17	0.26	2.35	0.01	0.00	0.01	0.00	26.78
24	19.10	4.88	0.30	0.61	1.91	0.08	0.00	0.02	0.01	26.91
26	18.99	5.02	0.11	0.37	2.19	0.03	0.00	0.01	0.00	26.73
28	19.26	4.78	0.18	0.39	1.97	0.01	0.00	0.00	0.01	26.62
29	18.90	5.04	0.18	0.44	2.27	0.02	0.01	0.02	0.00	26.88
30	19.25	4.71	0.18	0.46	2.06	0.00	0.02	0.00	0.01	26.69
31	19.42	4.61	0.16	0.39	1.92	0.02	0.00	0.01	0.01	26.55
32	18.92	5.11	0.24	0.34	2.21	0.00	0.00	0.00	0.00	26.82
33	18.88	5.13	0.20	0.30	2.23	0.01	0.02	0.02	0.01	26.79

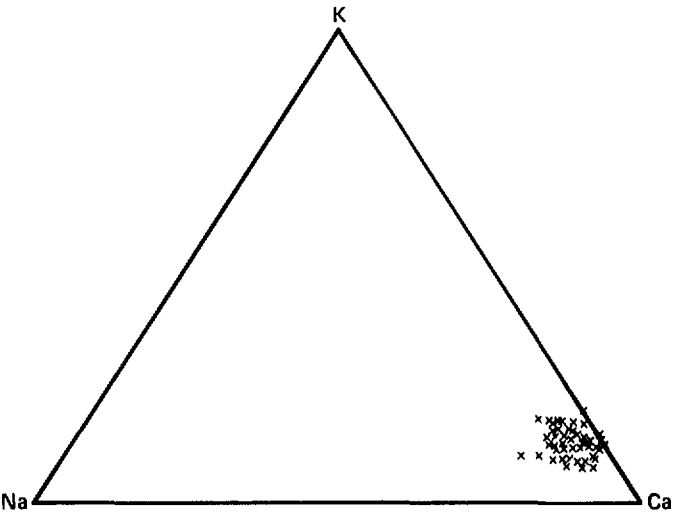

Figure D1. Ternary diagram (sodium-potassium-calcium) of calculated cation content based on 48 oxygens.

The silicon/aluminum ratio averaged 3.89 ± 0.17 and varied from 3.6 to 4.4 (Fig. D2). As Figs. D3(a) and D3(b) show, there was a weak inverse relationship between the silicon/aluminum and calcium and a much less clear direct relationship between the silicon/aluminum and potassium. These correlations cannot be used to argue strongly for some degree of substitution of sodium plus potassium plus silicon for calcium plus aluminum (Wise and Tschernich, 1978).

We investigated evidence for chemical zoning of calcium, potassium, and sodium within single grains of dachiardite by making WDS step-scan analyses. This was done by making simultaneous 15-s WDS counts over a 5-by-1-μ^2 area for calcium, potassium, and sodium, using three spectrometers and a rastered beam moved in 2 μ. The results of these scans, which were made both perpendicular to and parallel with the long dimension of large prismatic crystals, are shown in Fig. D4(a) and D4(b). With the exception of calcium near one edge of a crystal, there appeared to little chemical zoning within single crystals. The composition of the dachiardite crystals and the relative proportions of the cations remained constant despite a fluid phase whose composition evolved with time of reaction (see the main body of this report).

The dachiardite produced in those experiments appeared to have grown at the elevated temperature of the run, rather than during the vessel quench at the end of the run. Although no sample was taken of the quenched fluid that remained in the gold bag when the cell was disassembled following the 250°C runs, samples were taken after many of the 150 and 90°C experiments reported in the body of the text, as well as after the long-term experiments reported by Knauss et al. (1987). These fluids, which were quenched from the elevated temperature of the experiment to near room temperature while remaining in contact with the solids, all showed the same trends in composition. Invariably, potassium, aluminum, and pH decreased slightly while calcium and magnesium increased. The silicon and sodium concentrations appeared to have remained stable. However, a decrease in silicon that would be appropriate for the formation of a K-Al-clay would hardly be noticeable. The dachiardite produced in these experiments was calcium-rich; hence, the changes in solution composition caused by quenching the vessel could not have produced it. See the body of this report and the following sections of this appendix for additional details.

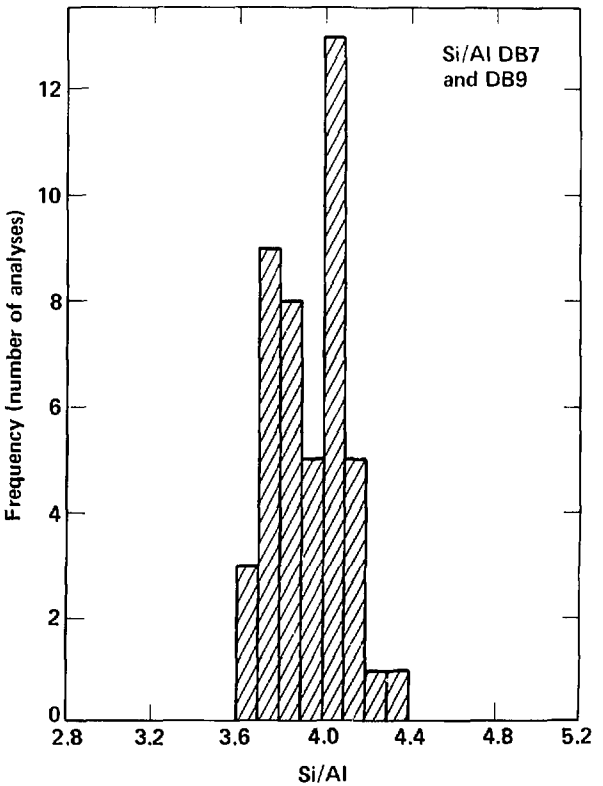

Figure D2. Histogram of silicon/aluminum ratio in dachiardite.

SEM Photographs and EDS Spectra of Dachiardite and Coexisting Mordenite

We used SEM observation and EDS spectra generated using a point electron beam to identify the secondary minerals formed as a result of the hydrothermal interaction of the tuff wafers with J-13 well water. The EDS spectra taken directly from the secondary minerals growing on the surface of the wafer showed the coexisting dachiardite and mordenite to be similar in composition. However, the dachiardite was always calcic (Fig. D5), while the mordenite contained subequal and varying amounts of alkali [Figs. D6(a) and D6(b)].

An abundant amount of dachiardite formed on the surface of the phenocrysts and on the fine-grained matrix (Fig. D7). In experiment D7, it was also found coating the surface of the titanium head inside the gold-bag reaction cell (Fig. D8). The dachiardite occurred most commonly as large, intergrown prismatic crystals with small, interpenetrating crystals growing at the preferred angle from the dominant faces (010) and (100) [Fig. D9(a)]. The prismatic dachiardite was well-terminated, usually by (001), (- 101), and (- 403). It also commonly formed rosettes of many prismatic crystals, some of which displayed reentrant angles, suggesting polysynthetic twinning [Fig. D9(b)]. Some crystal masses displayed both forms [D9(c)].

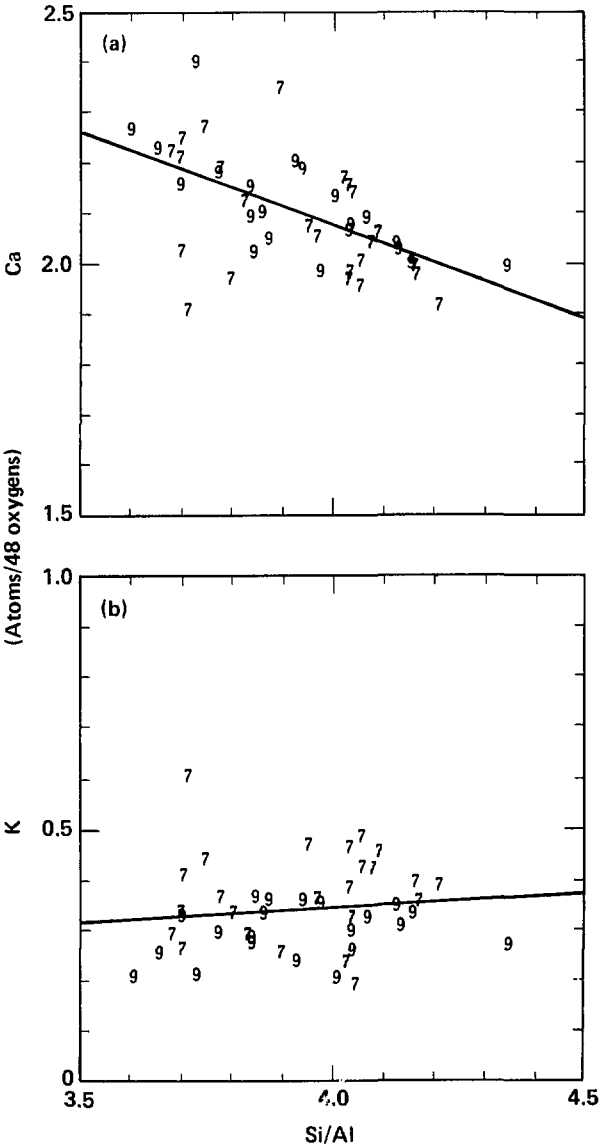

Figure D3. (a) Silicon/aluminum vs calcium shows an inverse relationship. (b) Silicon/aluminum vs potassium shows a weak positive relationship.

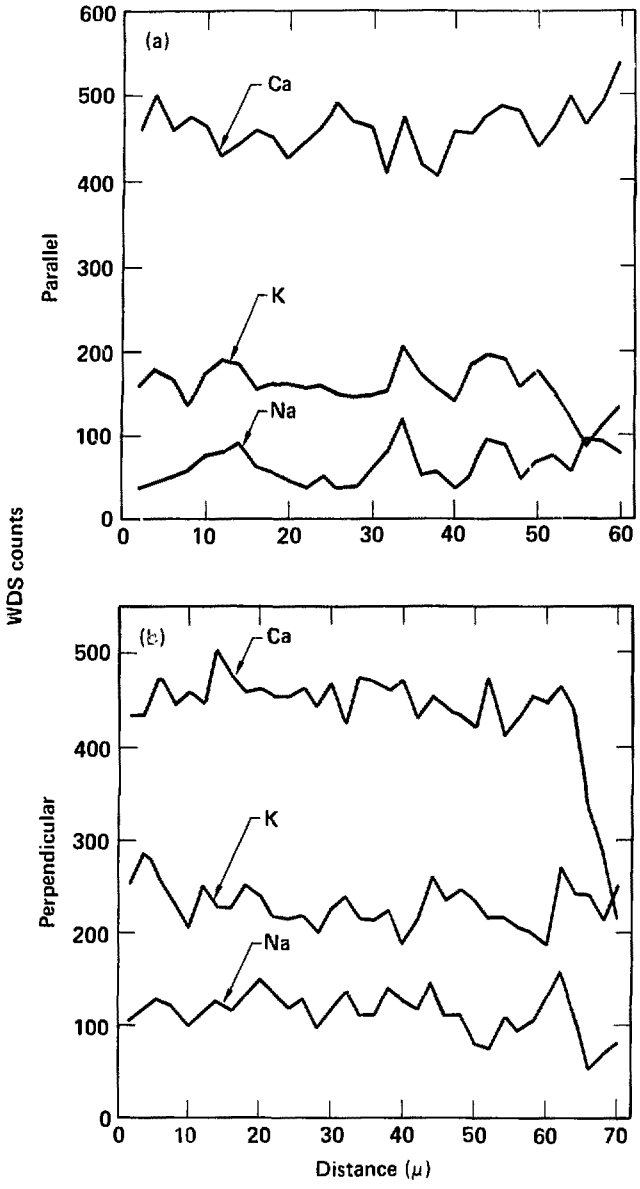

Figure D4. (a) WDS step-scan counts for calcium, potassium and sodium parallel to the long dimension of a single crystal of dachiardite. (b) WDS step-scan counts for calcium, potassium, and sodium perpendicular with the long dimension of a single crystal of dachiardite.

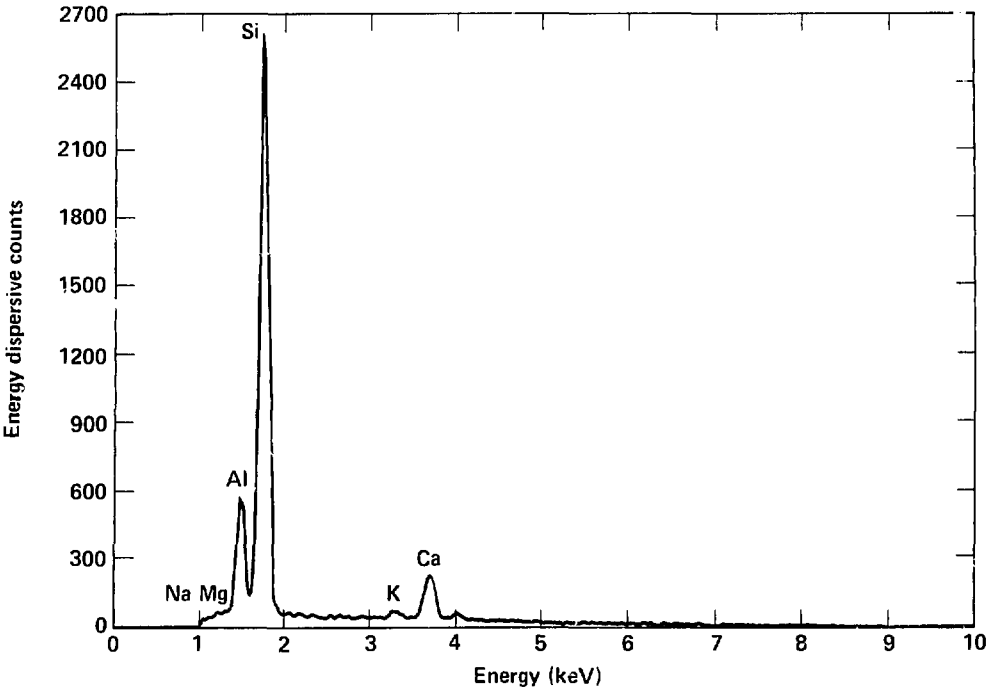

Figure D5. EDS spectra of dachiardite showing it to contain calcium with minor potassium and essentially no sodium or magnesium.

Less commonly, the crystals displayed a blocky form [Fig. D9(d)]. This latter form was seen by Barger et al. (1981) in dachiardite from Yellowstone. Coexisting mordenite was often intimately associated with the dachiardite, suggesting that the two zeolite minerals are obviously contemporaneous (Fig. D10).

Other run products formed in these experiments at 250°C were much less abundant than the dachiardite and included the minor claylike phases seen growing on the surface of the dachiardite crystals and a pure-silica phase that formed a perfect sphere (presumed to be cristobalite). Because the claylike phases were much less abundant and coated the dachiardite, and because the runs produced fairly alkaline *in situ* conditions (calculated *in situ* pH = 7.2 and neutral pH at 250°C = ~5.5), it is possible that the claylike phases were actually a product of the quench.

Generally speaking, conditions near neutral pH tend to favor the formation of phyllosilicates in which aluminum has a strong preference for sixfold coordination with oxygen, and silicon remains in tetrahedral coordination. As pH increases, layer silicates are displaced by tectosilicates (zeolites) in which both aluminum and silicon are tetrahedrally coordinated with oxygen (Barrer, 1981). These general arguments suggest that the zeolite dachiardite and mordenite are true run products, while the claylike phases are products of the quench. SEM photographs of these other secondary minerals seen on the wafers and EDS spectra generated from them may be found in Appendix E of this report.

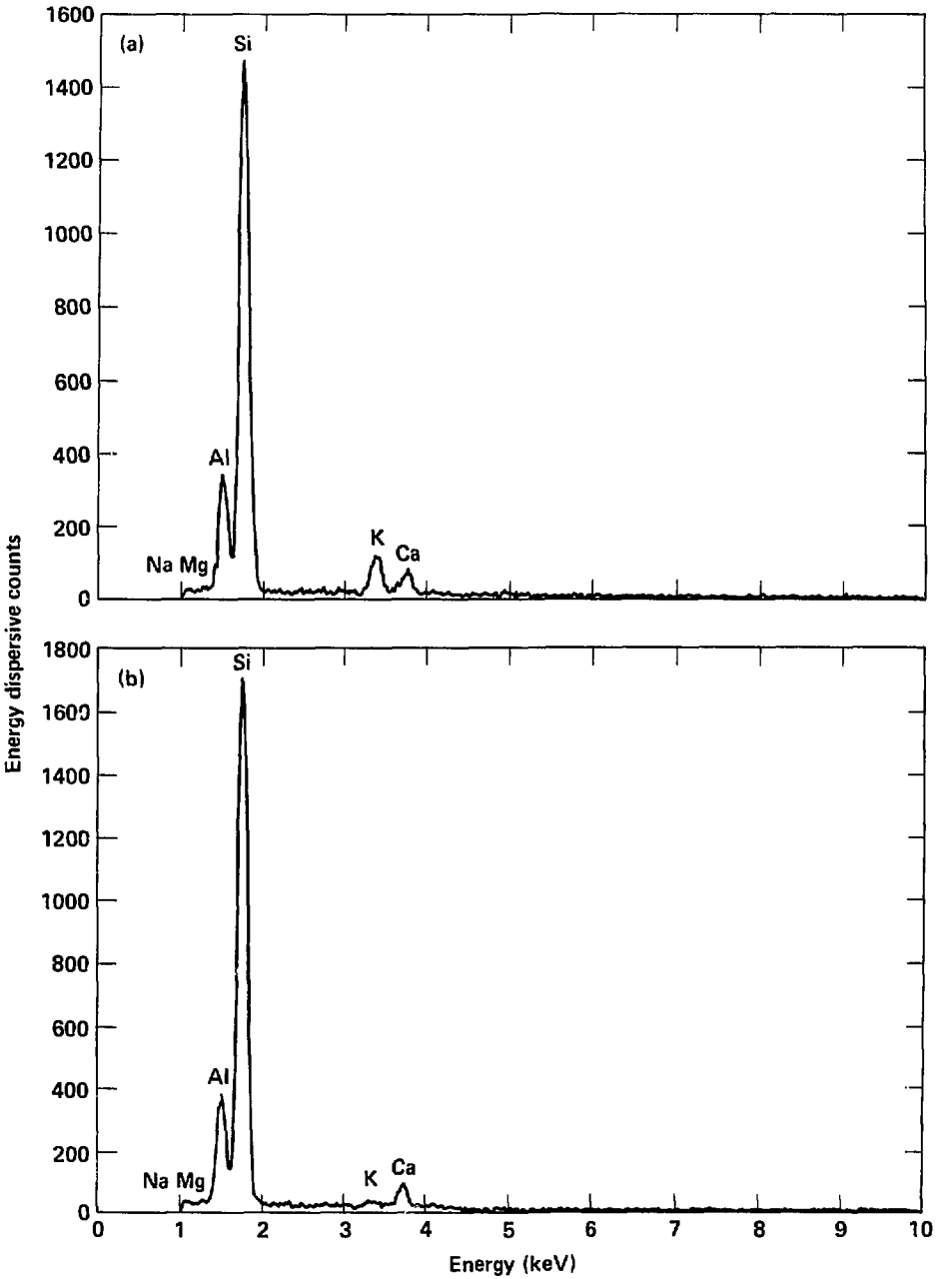

Figure D6. EDS spectra of mordenite (a and b) showing it to be more variable in composition, but invariably containing more potassium and sodium than the coexisting dachiardite (Fig. D5).

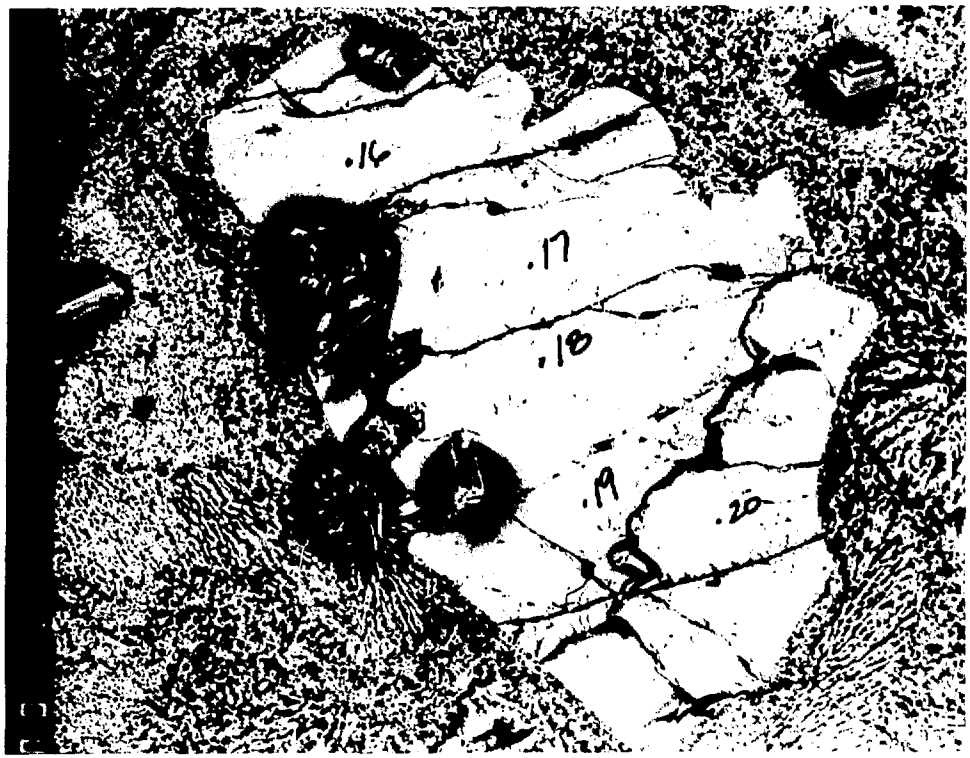

Figure D7. Dachiardite formed on the surface of phenocrysts as well as on the fine-grained matrix.

Figure D8. In experiment DB7 the dachiardite was also found coating the surface of the titanium head inside the gold-bag reaction cell.

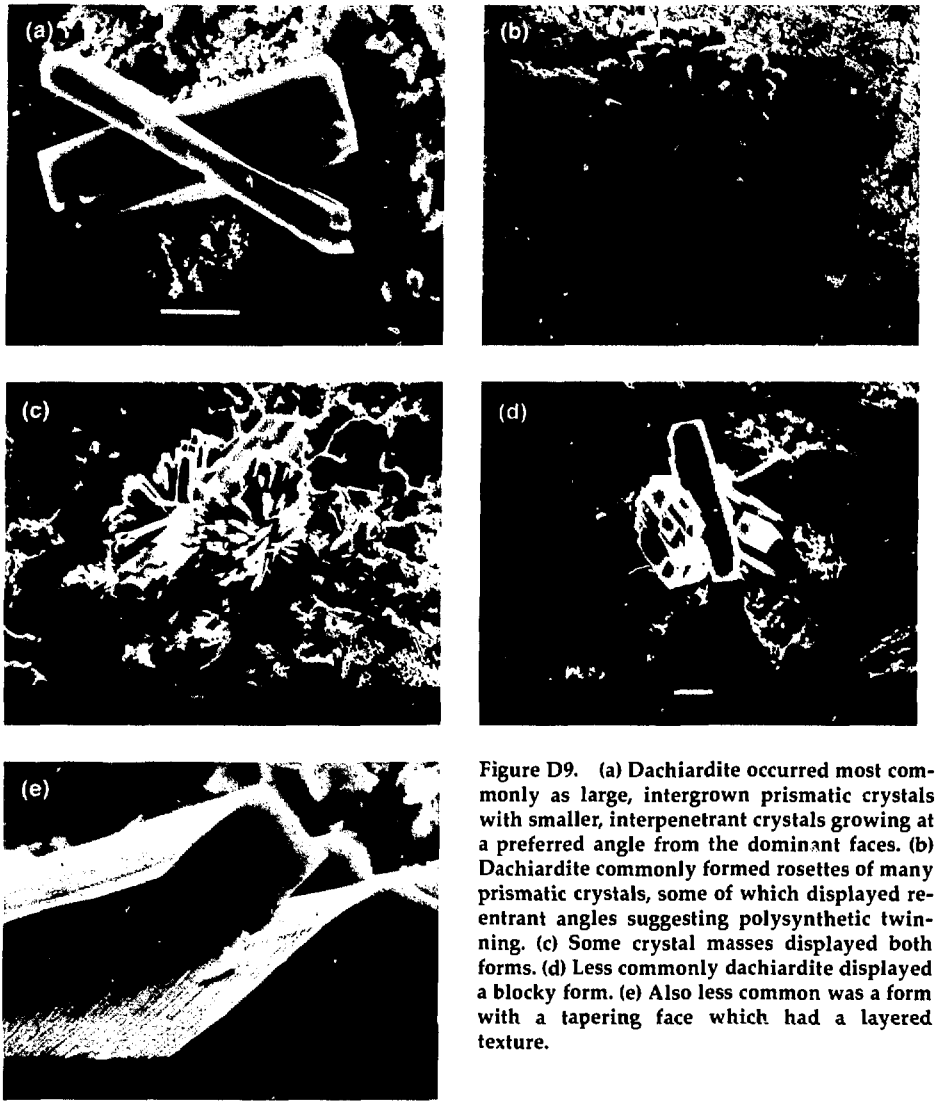

Figure D9. (a) Dachiardite occurred most commonly as large, intergrown prismatic crystals with smaller, interpenetrant crystals growing at a preferred angle from the dominant faces. (b) Dachiardite commonly formed rosettes of many prismatic crystals, some of which displayed reentrant angles suggesting polysynthetic twinning. (c) Some crystal masses displayed both forms. (d) Less commonly dachiardite displayed a blocky form. (e) Also less common was a form with a tapering face which had a layered texture.

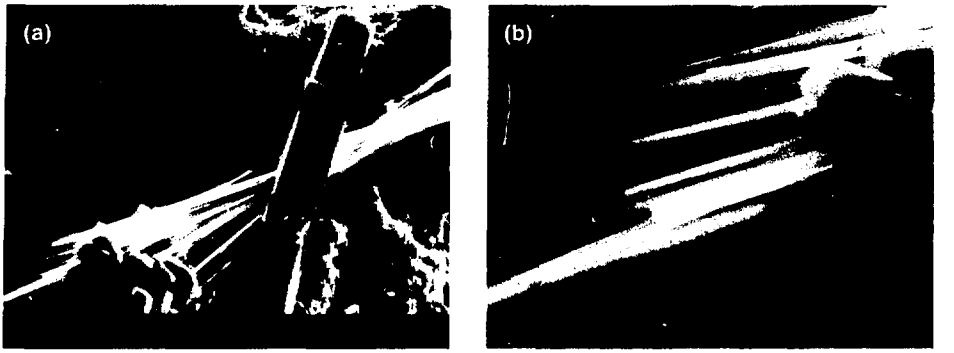

Figure D10. The coexisting mordenite was intimately associated with the dachiardite and the two zeolite minerals were obviously contemporaneous.

Conclusions

A rare, high-silica zeolite, dachiardite was formed by the hydrothermal interaction of a natural low-salinity ground water and a devitrified rhyolitic tuff. The solution from which the zeolite precipitated was well characterized and had a high silicon concentration that was maintained by the solubility of cristobalite. Under these experimental conditions, the composition of the dachiardite produced was closer to the calcium end member mineral than even the type locality mineral. The zeolite discriminated against both potassium and sodium in its growth and remained calcium-rich. No evidence for chemical zoning within the mineral was seen. When alkali substitution occurred, there was some evidence for corresponding silicon/aluminum substitution. Detailed SEM observation revealed the various crystal forms displayed by this mineral. The coexisting mineral assemblage (mordenite plus rare cristobalite and minor amounts of a potassium-bearing claylike phase) was also studied, although to a much lesser extent.

The formation of this or similar zeolites in the vicinity of a high-level waste package during the thermal period and its metastable persistence could have some beneficial effects with respect to radionuclide migration. Although the cation exchange properties of dachiardite are unknown, zeolites generally have good sorption capability. The thermal stability of dachiardite is also unknown, but experimental work suggests mordenite group zeolites are a higher temperature phase than the clinoptilolites-heulandites. This would argue for its continued metastable persistence in the near-field environment.

References

Alberti, A. (1975), "Sodium-Rich Dachiardite from Alpe di Suisi, Italy," *Contrib. Miner. Petrol.* **49**, 63–66.

Appleman, D. (1963), Least Squares Unit Cell Refinement Program, Prog. and Abstr., *Am. Cryst. Assoc. Mtg., Cambridge, MA.*

Barger, K. E. (1984), U.S. Geological Survey, Menlo Park, CA, personal communication.

Barger, K. E., and M. H. Beeson (1981), "Hydrothermal Alteration in Research Drill Hole Y-2, Lower Geyser Basin, Yellowstone National Park," Wyoming, *Am. Miner.* **66**, 473–490.

Barger, K. E., M. H. Beeson, and T. E. C. Keith (1981), "Zeolites in Yellowstone National Park," *Miner. Record*, 29–38.

Barrer, R. M. (1981), *Hydrothermal Chemistry of Zeolites* (Academic Press, NY), 78–80.

Bonardi, M. (1979), "Composition of Type Dachiardite from Elba: a Re-examination," *Miner. Mag.* **43**, 548–549.

Bonardi, M., A. C. Roberts, A. P. Sabina, and G. Y. Chao (1981), "Sodium-Rich Dachiardite from the Francon Quarry, Montreal Island, Quebec," *Can. Miner.* **19**, 285–289.

Gellens, L. R., G. D. Price, and J. V. Smith (1982), "The Structural Relationship Between Svetlozarite and Dachiardite," *Miner. Mag.* **45**, 157–161.

Knauss, K. G., W. J. Beiriger, and D. W. Peifer (1987), *Hydrothermal Interaction of Solid Wafers of Topopah Spring Tuff with J-13 Water at 90°C and 150°C Using the Dickson-Type Gold Bag Rocking Autoclaves: 2. Long-Term Experiments*, Lawrence Livermore National Laboratory, Livermore, CA, UCRL-53722.

Nishido, H., R. Otsuka, and K. Nagashima (1979), "Sodium-Rich Dachiardite from Chichijima, the Ogasawara Islands, Japan," *Bull. Sci. Eng. Res. Lab. Waseda U.*, **87**, 29–37.

Passaglia, E. (1970), "The Crystal Chemistry of Chabazites," *Am. Miner.* **55**, 1278–1301.

Wise, W. S., and R. W. Tschernich (1978), "Dachiardite-Bearing Zeolite Assemblages in the Pacific Northwest," *Natural Zeolites—Occurrence, Properties, Use*, L. B. Sand and F. A. Mumpton, Eds., (Pergamon Press, NY) 105–113.

Yoshimura, T., and S. Nakabayushi (1977), "Na-dachiardite and Associated High-Silica Zeolites from Tsugawa, Northeast Japan," *Sci. Rpts. Niigata U*, Series E, 49–65.

Appendix E. Secondary Mineral Energy-Dispersive Spectra, Semiquantitative Analyses, and Scanning Electron Microscope Photographs

Experimental Techniques

With the exception of the dachiardite produced in the two experiments run at 250°C, all secondary minerals produced as a result of the hydrothermal interaction of the natural ground water and the distilled water with tuff were too small and too rare to be physically removed from the surface of the wafer for detailed characterization. This meant that we could use only crystal habit (as observed by SEM) and approximate compositions (as determined by EDS spectra) to try to identify the run products. We also used a semiquantitative analysis of the EDS spectra to arrive at an approximation for the constituent oxides.

At best, the process of identification is very difficult. When run products are small (a few microns) or poorly crystalline, the unambiguous identification of secondary minerals is virtually impossible. Thus, we are limited to generating a list of potential minerals with no positive means of discrimination. Given the accelerating voltage (15 kV) used in this analysis and the densities of the minerals under investigation, we are producing an x-ray signal from a depth on the order of a few microns within the sample. Focusing the electron beam on a 1- or 2-μ-diam secondary mineral that is growing on the surface of the wafer will obviously result in x rays being generated from the underlying wafer, as well as from the secondary mineral itself. In the case of poorly crystalline or run products, we can gain no information about crystal habit that might aid in its identification. These are the limitations under which the post-test characterization of secondary minerals was undertaken.

Despite the above limitations, we were able to obtain some information about the identity of the run products produced in the 250 and 150°C hydrothermal experiments. To minimize the effects of the electron beam on the secondary minerals that were growing on the surface of the wafer, we used a defocused beam when possible, dropped the beam current to minimize the loss of volatiles (H_2O) and alkalis, and kept the count time used to gather EDS spectra to a minimum (usually about 5 s).

In addition to identifying the elements in each spectra by their x-ray energy, we used a semiquantitative reduction of the EDS spectra to estimate the concentration of constituent oxides. The spectral data reduction was performed with a semiquantitative analysis subroutine (SSQ) of the SANDIA TASK-84 software package. This package for stage and spectrometer automation, data acquisition, and data reduction was written for the electron microprobe (Chambers, 1984).

The routine procedure for the post-test analysis of run products consisted of the following steps. First, we used the SEM on the JEOL 733 EMP to scan the entire surface of the wafer at moderate magnification (between 500 and 1000 ×) to locate run products of a micron or larger. We then examined specific areas of interest in more detail at higher magnification. SEM photos were taken and EDS spectra were collected. The spectra were then plotted on an HP plotter and the SSQ semiquantitative analysis performed, based on a deconvolution of the EDS spectra. When we needed more detailed SEM photography, we noted the locations of areas of interest on the wafer and then photographed those areas using an AMR 1000 SEM. We use this instrument exclusively for SEM photography and keep it finely tuned for this purpose. Conversely, we use the EMP primarily for WDS quantitative analysis, and it is set up to maximize its performance as an analytical instrument. Hence, its resolution and performance in taking SEM photos is compromised.

Secondary Run Products Identified in the 250°C Experiments (DB7 and DB9)

The dominant secondary mineral produced in these hydrothermal experiments was the zeolite, dachiardite. It is characterized in Appendix D, which includes SEM photos of dachiardite and the coexisting mordenite. Appendix D also contains some EDS spectra for these minerals. The SSQ analyses of the

EDS spectra for dachiardite (Fig. D5) and mordenite (Fig. D6) are given in Tables E1–E3, respectively. Because XRD gave us an unambiguous identification of the dachiardite, we will not give any further attention to this run product in this appendix.

We identified the other zeolite seen in experiment DB9 as mordenite based on its EDS spectra, the SSQ analysis, and its crystal habit as seen in SEM photos. The composition of mordenite is nominally

$$(Na_2,K_2,Ca)\,[Al_2Si_{10}O_{24}] \cdot 7H_2O$$

From the EDS spectra measured in this experiment, the composition is variable, but the typical spectra are either calcium- or potassium-rich with a high silicon/aluminum ratio; sodium is never the dominant cation. The common form of mordenite is an extremely delicate fiber with a length-to-width ratio of 100 or more. The zeolite seen in Fig. D10 and in Figs. E1 through E3 display these characteristics. Unfortunately, the zeolites mordenite and erionite both occur in these forms, and it is difficult to distinguish them in SEM photos. However, mordenite and erionite rarely occur together (Mumpton and Ormsby, 1976), whereas dachiardite and mordenite almost invariably occur together (Wise and Tschernich, 1978). On the basis of all the above indirect evidence, we tentatively identify the secondary zeolite in experiment DB9 as mordenite.

The other run products seen at this temperature were a poorly crystalline, potassium-bearing clay-like phase (Fig. E4) and a pure silica phase (Fig. E5). Both of these phases were very rare. The pure silica phase is forming a perfect sphere, which is a form displayed by cristobalite. Within the first two weeks in both experiments a dissolved silicon concentration approximately equal to cristobalite solubility was reached and maintained for the remainder of the run. The clay-like phase only occurs covering the other secondary minerals, suggesting that it formed later in the experiment. It may simply be a product of the quench. Further experimental work will be required to address this question. An unambiguous identification of either of these phases is not possible based on SEM morphology or composition as estimated from their EDS spectra.

An additional run product was seen only in the experiment (DB7) with outcrop tuff (Fig. E6). These appeared to be calcite rhombs, although they were badly etched (in some cases only shells remained) and contained significant silicon. Tentatively we consider these to be calcite remaining from an earlier episode of calcite deposition that occurred when the solution was briefly supersaturated with respect to calcite. Modeling these experiments with EQ3/6 (Delany, 1985) lends some support to this conjecture.

Secondary Run Products Identified in the 150°C Experiments (DB6 and DB8)

As mentioned in the text, the run products at this lower temperature were less well developed, poorly crystalline and much less abundant than at 250°C. Because none were larger than about 10 μ, we could not repeat the detailed characterization that we did with the zeolite produced at the higher temperature. The identity of these run products may only be inferred from their EDS spectra and morphology; an

Table E1. SSQ semiquantitative analysis of EDS spectra in Fig. D5.

Element	Wt %	Oxide	Wt %
Si	45.5	SiO_2	81.2
Al	6.7	Al_2O_3	10.5
Ca	4.9	CaO	5.7
K	1.0	K_2O	1.0
Na	0	Na_2O	0
Mg	0	MgO	0
Fe	0	FeO	0
O	40.7		

Table E2. SSQ semiquantitative analysis of EDS spectra in Fig. D6(a).

Element	Wt %	Oxide	Wt %
Si	45.6	SiO_2	81.2
Al	7.0	Al_2O_3	11.0
Ca	2.7	CaO	3.1
K	4.6	K_2O	4.5
Na	0	Na_2O	0
Mg	0	MgO	0
Fe	0	FeO	0
O	40.1		

Table E3. SSQ semiquantitative analysis of EDS spectra in Fig. D6(b).

Element	Wt %	Oxide	Wt %
Si	47.3	SiO_2	83.4
Al	6.5	Al_2O_3	10.1
Ca	3.0	CaO	3.4
K	0.8	K_2O	0.8
Na	1.9	Na_2O	2.1
Mg	0	MgO	0
Fe	0	FeO	0
O	40.4		

Figure E1. A sheaf of mordenite fibers from experiment DB9 (250°C).

unambiguous identification is not possible. They are thought to include potassium-, calcium-, magnesium-, and/or iron-bearing clay-like phases, boehmite (or gibbsite), and cristobalite. Examples of the potassium-bearing clay-like phase and its EDS spectra are shown in Fig. E7. An example of the boehmite (or possibly gibbsite) is shown in Fig. E8(a) and the EDS spectra in Fig. E8(b). Between approximately 150 and 300°C, the stable aluminum hydroxide phase should be boehmite. The pure silicon phase is shown in Fig. E9. Note that the form (a perfect sphere) is identical to that seen at the higher temperature. In these experiments at 150°C the dissolved silicon concentration is also approximately equivalent to that of cristobalite solubility.

In the experiment run with outcrop tuff an additional phase seen was calcite, as shown in Fig. E10(a), with its EDS spectra in Fig. E10(b) (see Table E4 for SSQ semiquantitaive EDS analysis). The calcite produced in this experiment (DB6) is distinctly less etched than that in the outcrop tuff experiment at 250°C, which also produced some calcite, and it has significantly less silicon associated with it.

Figure E2. A high magnification view of the bladed nature of the mordenite fibers. Contrast this with the typical hexagonal form of the needles displayed by erionite, a zeolite that also occurs in fibers (250°C).

Secondary Run Products Identified in the 90°C Experiment (DB14) and the Experiments at 150°C and 90°C Run in Distilled Water (DB16 and DB17)

Despite our efforts to locate any secondary minerals growing on the surface of these three drillcore wafers, we did not see any. We have not planned any additional experiments that call for leaching in distilled water. However, we have recently completed two long-term experiments (303 days) using drillcore tuff wafers reacted with J-13 water at 90 and 150°C. With the longer reaction times it may be possible to identify secondary minerals produced at the lower temperature. The results of these long-term experiments will be presented in Knauss et al. (1987).

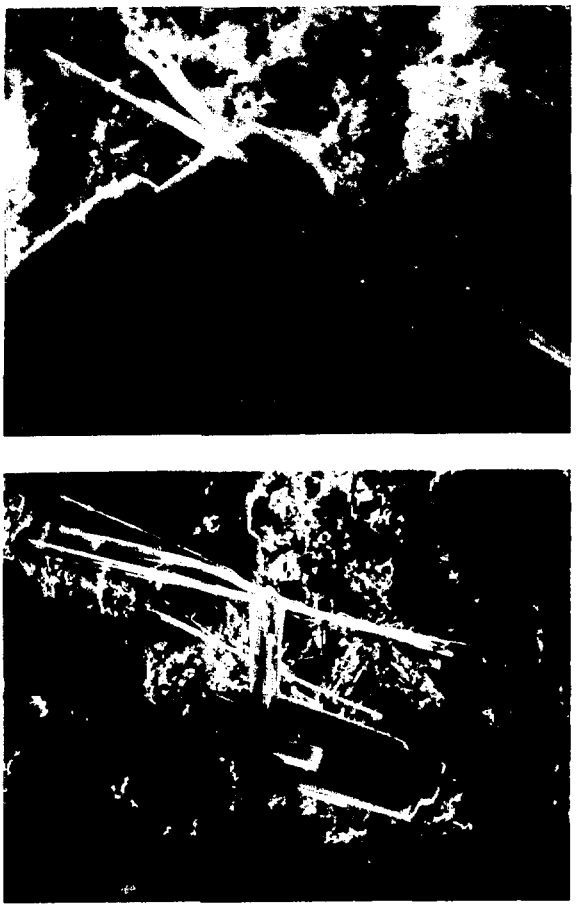

Figure E3. These photos illustrate the delicate nature of the mordenite fibers (250°C).

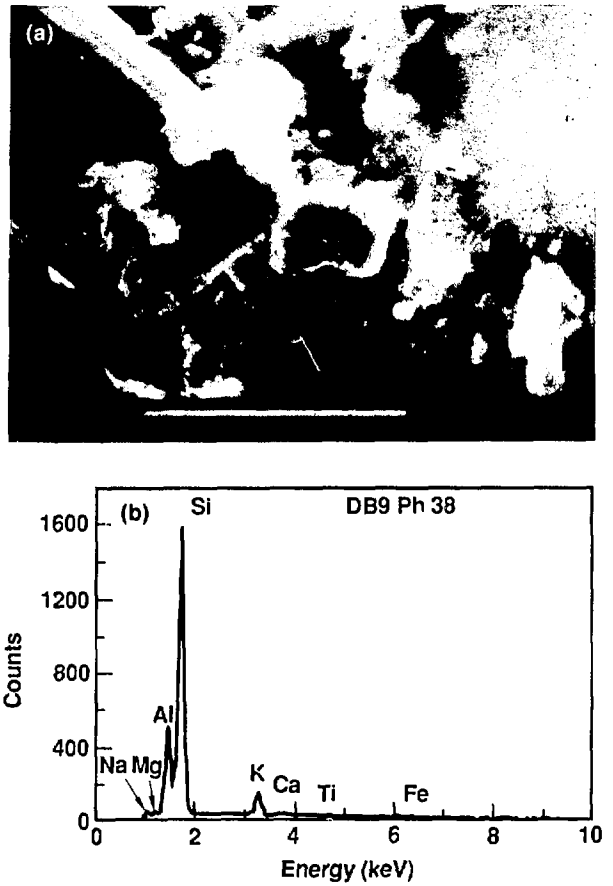

Figure E4. (a) A relatively rare, potassium-bearing, clay-like phase seen covering the other secondary minerals. It may be a product of the quench. (b) EDS spectra of the run product shown in (a) (250°C).

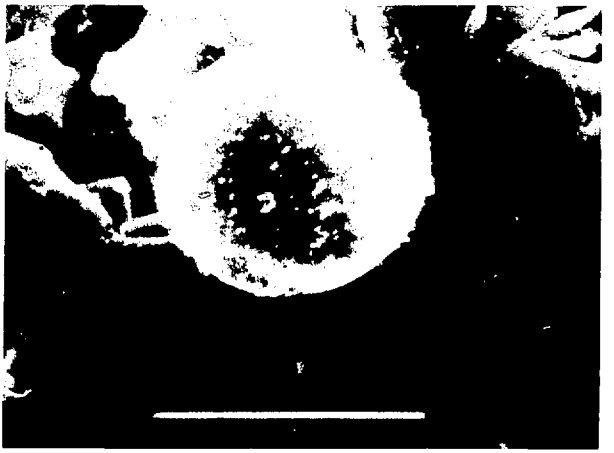

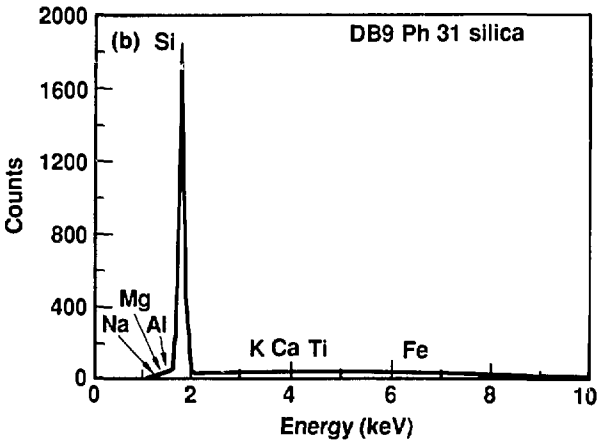

Figure E5. (a) A very rare pure silica phase that we tentatively identify as cristobalite. See text for details. (b) EDS spectra of the run product seen in (a) (250°C).

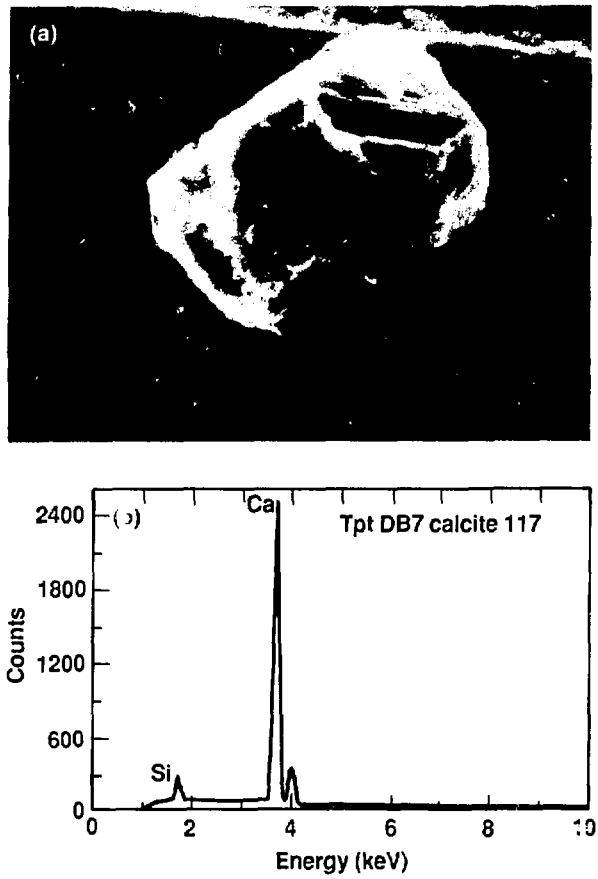

Figure E6. (a) One additional run product seen in the experiment with outcrop tuff. We tentatively identify it as calcite, which occurs as a relic from earlier solution conditions. It is actively dissolving. (b) EDS spectra of the run product seen in (b) (250°C).

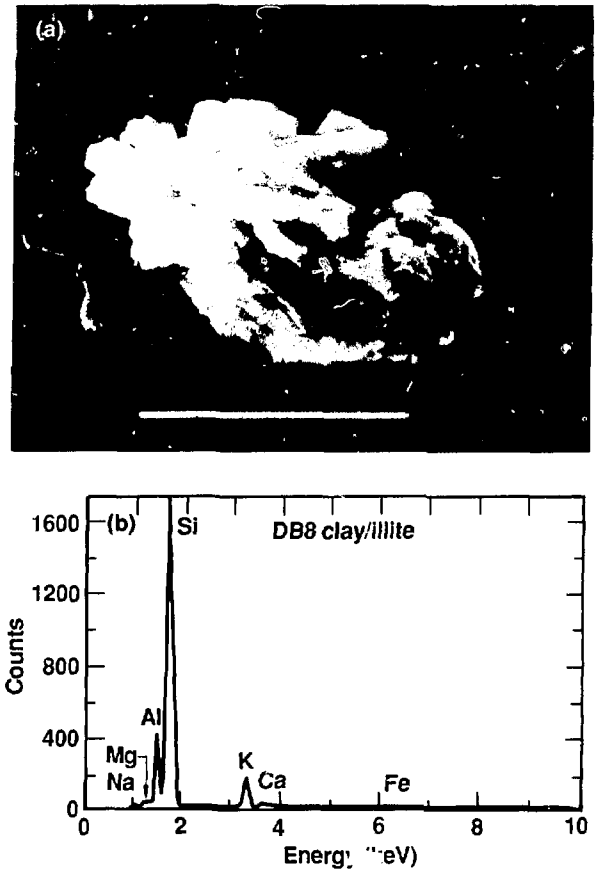

Figure E7. (a) An example of the potassium-bearing, clay-like phase seen in experiment DB8. (b) EDS spectra of the run product seen in (a) (150°C).

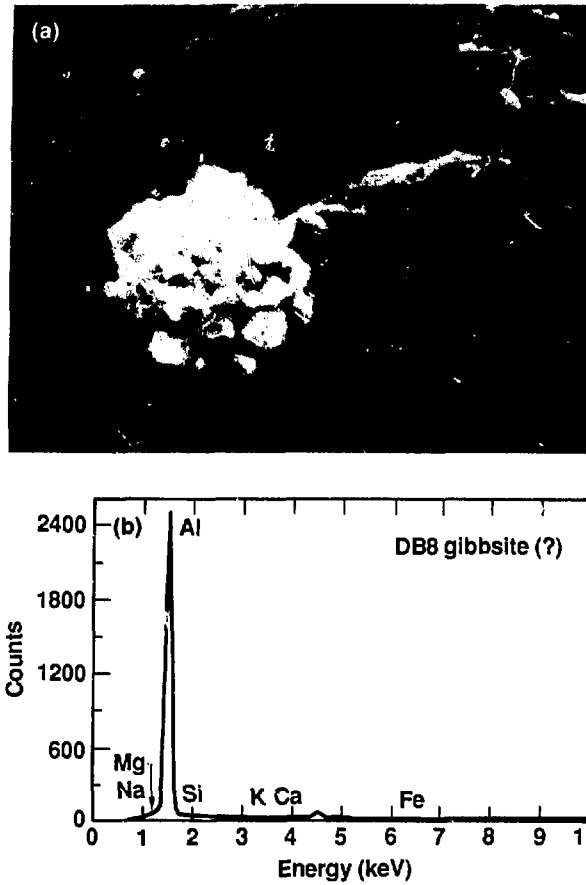

Figure E8. (a) The cluster of small (<1 μ) crystals is a pure aluminum phase, probably boehmite. (b) EDS spectra of the run product seen in (a) (150°C).

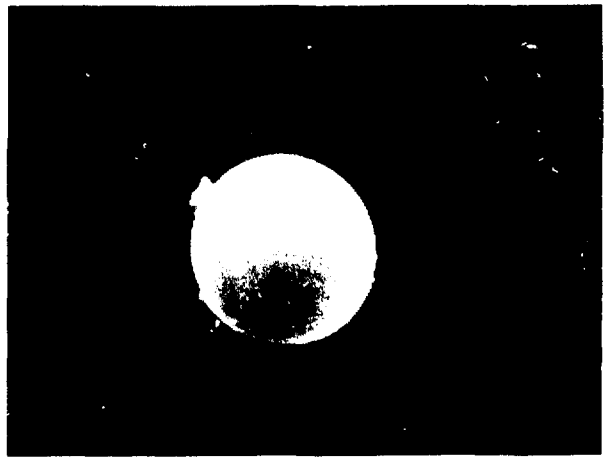

Figure E9. A very rare pure silica phase, which we tentatively identify as cristobalite.

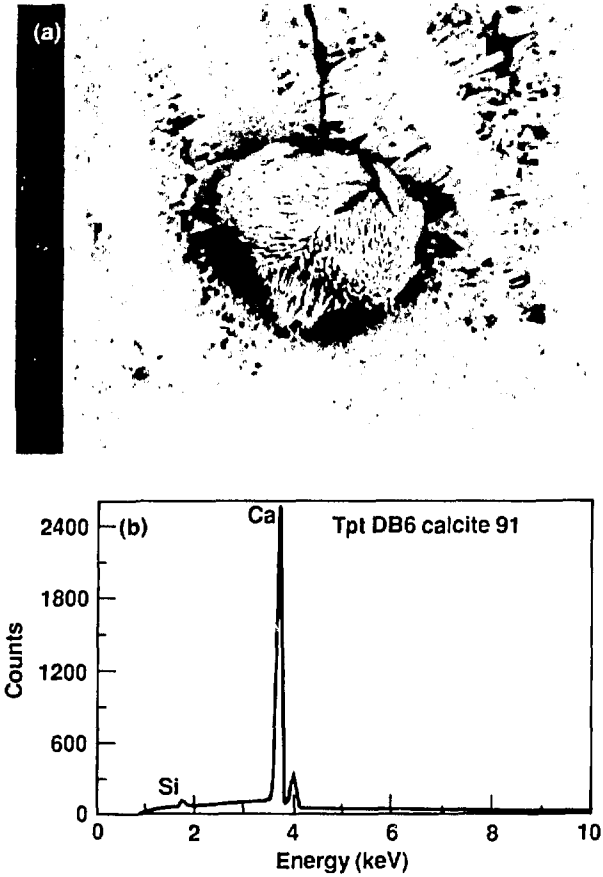

Figure E10. (a) One additional run product seen in the outcrop tuff experiments at 150°C was a phase that we tentatively identify as calcite. EDS spectra of the run product seen in (a) (150°C).

Table E4. SSQ semiquantitative analysis of EDS spectra in Fig. E6(b).

Element	Wt %	Oxide	Wt %
Si	0.8	SiO_2	1.5
Al	0	Al_2O_3	0
Ca	72.3	CaO	98.4
K	0	K_2O	0
Na	0	Na_2O	0
Mg	0	MgO	0
Fe	0	FeO	0
O	27.0		

References

Chambers, W. F. (1984), Sandia National Laboratories, Livermore, CA, personal communication.

Delany, J. M. (1985), *Reaction of Topopah Spring Tuff with J-13 Water: A Geochemical Approach Using the EQ3/6 Reaction Path Code*, Lawrence Livermore National Laboratory, Livermore, CA, UCRL-53631.

Knauss, K. G., W. J. Beiriger, and D. W. Peifer (1987), *Hydrothermal Interaction of Solid Wafers of Topopah Spring Tuff with J-13 Water at 90°C and 150°C Using the Dickson-Type Gold Bag Rocking Autoclaves: 2. Long-Term Experiments*, Lawrence Livermore National Laboratory, Livermore, CA, UCRL-53722.

Mumpton, F. A., and W. C. Ormsby (1976), "Morphology of Zeolites in Sedimentary Rocks by Scanning Electron Microscopy," *Clays Clay Mineral.* **24**, 1–23.

Wise, W. S., and R. W. Tschernich (1978), "Dachiardite-Bearing Zeolite Assemblages in the Pacific Northwest," *Natural Zeolites—Occurrence, Properties, Use*, L. B. Sand and F. A. Mumpton, Eds. (Pergamon Press, New York), 105–113.